

Spatially uniform and nonuniform analyses of electroencephalographic dynamics, with application to the topography of the alpha rhythm

S. C. O'Connor and P. A. Robinson

*School of Physics, University of Sydney, Sydney, New South Wales 2006, Australia
and Brain Dynamics Center, Westmead Hospital, Westmead, New South Wales 2145, Australia*

(Received 18 January 2004; published 21 July 2004)

Corticothalamic dynamics are investigated using a model in which spatial nonuniformities are incorporated via the coupling of spatial eigenmodes. Comparison of spectra generated using the nonuniform analysis with those generated using a uniform one demonstrates that, for most frequencies, local activity is only weakly dependent on activity elsewhere in the cortex; however, dispersion of low-wave-number activity ensures that distant dynamics influence local dynamics at low frequencies (below approximately 2 Hz), and at the alpha frequency (approximately 10 Hz), where propagating signals are inherently weakly damped, and wavelengths are large. When certain model parameters have similar spatial profiles, as is expected from physiology, the low-frequency discrepancies tend to cancel, and the uniform analysis with local parameter values is an adequate approximation to the full nonuniform one across the whole spectrum, at least for large-scale nonuniformities. After comparing the uniform and nonuniform analyses, we consider one possible application of the nonuniform analysis: studying the phenomenon of occipital alpha dominance, whereby the alpha frequency and power are greater at the back of the head (occipitally) than at the front. In order to infer realistic nonuniformities in the model parameters, the uniform version of the model is first fitted to data recorded from 98 normal subjects in a waking, eyes-closed state. This yields a set of parameters at each of five electrode sites along the midline. The inferred parameter nonuniformities are consistent with anatomical and physiological constraints. Introducing these spatial profiles into the full nonuniform model then quantitatively reproduces observed site-dependent variations in the alpha power and frequency. The results confirm that the frequency shift is mainly due to a decrease in the corticothalamic propagation delay, but indicate that the delay nonuniformity cannot account for the observed occipital increase in alpha power; the occipital alpha dominance is due to decreased cortical gains and increased thalamic gains in occipital regions compared to frontal ones.

DOI: 10.1103/PhysRevE.70.011911

PACS number(s): 87.19.La, 87.18.Bb, 87.10.+e, 87.18.Hf

I. INTRODUCTION

In the present work we compare uniform and nonuniform analyses of electroencephalographic (EEG) activity. Frequency EEG spectra are known to differ significantly across the head [1,2], indicating that the underlying physiological parameters may be inherently dependent on position. However, work using a spatially uniform version of the model has been successful in predicting the form of individual EEG spectra, including the spectral peaks such as the alpha rhythm [3]. The model predicts that the alpha rhythm is generated in feedback loops between the cortex and the thalamus, and that changes in the relative strengths of these loops are largely responsible for determining the reactivity of the alpha rhythm; for example, its diminished amplitude upon eye opening, or drowsiness [3]. Indeed, a key advantage of the model is its ability to unify large-scale cortical activity of many different types into a single framework. For example, the model has predicted trends seen in various states of arousal [3], certain seizure onsets and dynamics [4], and evoked response potentials [5]. In the spatial domain, it has successfully addressed coherence and correlations [6], as well as unifying wave-number spectra recorded from the scalp [7], the cortex [8], and as evoked response potentials [9].

This model has been recently generalized to incorporate spatial nonuniformities in the parameters, so that site-

dependent variations in EEG spectra can be investigated [10]. It was shown that mode splitting due to a spatial nonuniformity in the corticothalamic loop delay could explain the phenomenon of split alpha peaks, observed in a significant percentage of individuals; that is, the corticothalamic loop delay varies spatially across the head. This is distinct from previously postulated explanations for split alpha, such as numerous spatially discrete pacemakers [11,12], or purely cortical spatial eigenmodes [12].

In the present work, we compare the predictions of our spatially uniform and nonuniform models. In Sec. II A we outline the nonuniform version of the model in which the parameters can vary across the brain, and the ensuing spectrum is calculated from the resulting coupled spatial eigenmodes. In this formalism, a localized parameter variation can affect the spectrum at distant sites on the cortex. The present work has three main aims, the first of which is to determine the extent to which spatial nonuniformities in cortical parameters affect the locally measured activity. The uniform model assumes that activity at each electrode can be approximated as being independent of activity at other electrodes: the validity of this approximation is tested in Sec. III by comparing the local effective value (LEV) and nonuniform models for various spatial profiles of the parameters. In this way, we can determine the circumstances in which the fully nonuniform version must be used to adequately model the brain dynamics, and for which cases the uniform model is sufficient.

The second aim is to estimate likely spatial profiles for the model parameters along the midline, from the front to the back of the head. We explore the front-to-back variations only, because these are thought to be greater than the relatively symmetrical left-to-right variations [1], and suffice to establish the main effects. The present study thus analyzes one-dimensional nonuniformities in a two-dimensional cortex; a more complete analysis incorporating two-dimensional parameter nonuniformities will be the subject of future work. Likely parameter variations in one dimension are explored in Sec. IV, in which a Levenberg-Marquardt nonlinear least squares optimization routine is used to fit the uniform version of the model to spectral data recorded from 98 normal subjects. This inverse modeling is performed for each subject at five midline electrode sites to ascertain likely front-to-back variations in the model parameters.

The third aim of this work is to implement the nonuniform model to study one possible application: the phenomenon of occipital dominance of the alpha rhythm. This is addressed in Sec. V, by applying the inferred parameter nonuniformities from the inverse modeling to the nonuniform mode-coupling model. The alpha rhythm has a frequency of approximately 10 Hz and is prevalent in relaxed, awake subjects with closed eyes. It has largest amplitude at the very back of the head, in occipital regions and, to a lesser extent, the surrounding parietal and posterior temporal regions [1]. There is some debate as to whether similar rhythms towards the front of the head can be classified as alpha, since they are usually of lower amplitude and have slightly different frequency (usually 0.5–1.0 Hz lower) than the dominant occipital rhythm [1].

Some studies have correlated occipital alpha dominance with cortical and subcortical activity by using electroencephalography (EEG) in conjunction with positron emission tomography (PET) [13–15], and functional magnetic resonance imaging (fMRI) [16]. The results of the correlative studies are somewhat contradictory, with authors variously reporting that alpha dominance is correlated with either increased [15,16] or decreased [13,14] thalamic activity. In the present work, we address these contradictions using our spatially nonuniform model. The use of a physiologically based model to elucidate the mechanism responsible for occipital alpha dominance removes the limitations of correlative studies, such as the above, which are unable to distinguish between causally and noncausally correlated phenomena [16]. The model is thus able to provide direct insight into the physiological and anatomical generators of the alpha rhythm.

II. MODELS

We draw the reader's attention to three distinct versions of the model used in this paper, each of which incorporates a different level of spatial nonuniformity in the parameters. The three models can be understood by referring to Fig. 1, which shows the variation of an arbitrary parameter across the head, where we place the front of the head at $d=0$ m. The solid line in Fig. 1 represents the actual variation of the parameter; this was chosen arbitrarily for Fig. 1, and is for illustrative purposes only. The first version of the model is

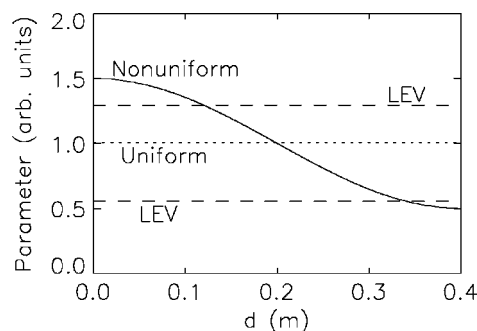


FIG. 1. Schematic comparison of approximations to parameter variations in the three versions of the model used in the paper. The nonuniformity of an arbitrary parameter is shown as a function of position on the head. The solid line shows the actual nonuniformity in the parameter, as well as the values it would take using the nonuniform model. The dotted line shows the value the parameter would take using the global uniform model; it is the average value over the head. The dashed lines show the value the parameter would take using the local effective value (LEV) model; the values are shown for two different positions on the head, at $d=0.1$ m and at $d=0.4$ m. Note that the effective value at a given point on the head is generally not the same as the actual value at that point; it is displaced towards the global mean value.

represented by the dotted line in Fig. 1. It is uniform, and does not allow for spatial variations in the model parameters under any circumstances. The parameters are set to their global mean values, and never vary from these. We shall henceforth refer to this version as the global uniform model. For the example in Fig. 1, this global model would give a good approximation to the power spectrum near the middle of the head ($d=0.2$ m), and worse approximations elsewhere.

The second version of the model is represented by the dashed lines in Fig. 1. This model is also uniform for any given situation, and does not allow for spatial variations in the model parameters. In this case, however, the uniform values of the parameters are chosen according to the location of interest on the head, in order to best match the actual local spectrum to the set of possible uniform-parameter ones. For example, when investigating activity at the front of the head, a different set of uniform parameters will be used than when investigating activity at the back. Thus this version uses the best uniform set of parameters for each location on the head. Examples of two different sets of uniform values are represented by the two dashed lines in Fig. 1, which represent the “best” effective uniform values at $d=0.1$ m and at $d=0.4$ m, respectively. Note that the best effective value at a given point is not necessarily the same as the actual value of the parameter at that point, since the spectrum is influenced by surrounding regions via wave dispersion. In general, the effective local value is displaced towards the mean value compared to the actual local value. We shall henceforth refer to this model as the local effective value (LEV) model. This model gives a good approximation to the power spectrum at a given point on the head, and worse approximations elsewhere.

The third version of the model used in this paper is fully nonuniform, and allows for spatial nonuniformities in the model parameters; it is shown by the solid line in Fig. 1,

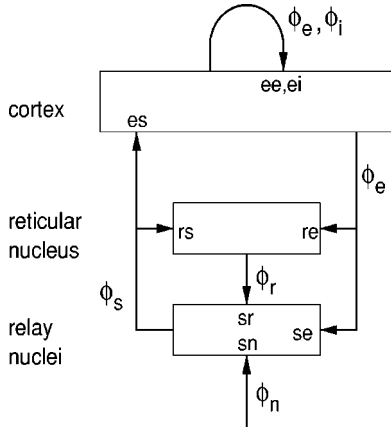


FIG. 2. Diagram of corticothalamic connections showing the cortex, reticular nucleus, and relay nuclei. The cortex is extensively connected to itself, and also projects to and receives projections from the thalamus. There are two loops through the thalamus: a direct loop passing only through the relay nuclei, and an indirect loop which also passes through the reticular nucleus. There is also an intrathalamic loop. Corticothalamic gains are indicated on the diagram.

which also represents the actual nonuniformity of the parameter in this case. We shall refer to this as the nonuniform model. This version of the model gives a good approximation to the power spectrum everywhere on the head simultaneously.

The first two versions of the model, both of which are essentially spatially uniform, have been used extensively to explore numerous phenomena, as mentioned in Sec. I. These are both analytically tractable and computationally light. The third, fully nonuniform, version, is more general than the earlier versions, at the cost of increased computational requirements and loss of analytical tractability in most cases. One aim of the present work is to determine under which circumstances the uniform LEV model is sufficient to accurately describe the dynamics, and in which cases the analytically intractable nonuniform model must be used.

A. Nonuniform model

In this section we summarize the nonuniform corticothalamic model, which has been recently generalized to incorporate spatial nonuniformities via coupling of eigenmodes. The full details and justification of the model can be found elsewhere [10]. We review the full two-dimensional (2D) model, in which the cortex is modeled as a thin, continuous, bounded sheet. Precise boundary conditions prove not to be very important in determining activity in this model [6,17,18], so the detailed geometry of cortical convolutions is ignored. The corticothalamic connectivity assumed in the model is shown in Fig. 2, incorporating the relay nuclei s , which relay subthalamic input ϕ_n to the cortex, and feed cortical signals back to the cortex; the thalamic reticular nucleus r , which inhibits the relay nuclei; and the cortex, which contains both excitatory e and inhibitory i neurons, receives projections from the relay nuclei, projects to both

the reticular and relay nuclei, and is densely connected to itself.

The continuum treatment of the cortex implies that the firing rate of signals emitted by single excitatory or inhibitory neurons, which depend on their individual cell body potentials, are averaged to give mean values of the outgoing pulse field $\phi_a(\mathbf{r}, t)$, where $a=e, i$. The mean rate of generation of neuronal pulse density depends on the mean local cell-body potential via a smooth sigmoidal function that increases from 0 to its maximum value as the potential increases from $-\infty$ to ∞ . We approximate the sigmoidal function here by a linear function on the assumption that deviations from the steady state are small at large scales in normal, nonseizure states. This approximation has been found to yield excellent agreement with observed frequency spectra and other phenomena, as mentioned in Sec. I.

The local mean cell body potential of neurons of type a in the cortex is a function of inputs from other cortical neurons, and from excitatory subcortical neurons. Incoming activity is received in the dendritic tree and filtered as it spreads along the dendrites to the cell body. The quantity L_{ab} is a dendritic low-pass filter function which accounts for the temporal delay and smearing of an incoming signal from a neuron of type $b=e, i, s$ as it travels along the dendritic tree to the cell body of a neuron of type $a=e, i$. It can be written [19]

$$L_{ab}(\mathbf{r}, \omega) = \frac{1}{[1 - i\omega/\alpha(\mathbf{r})][1 - i\omega/\beta(\mathbf{r})]}, \quad (1)$$

where β and α are the inverse rise and decay times of the dendritic potential, respectively.

Outgoing pulses from each neuron propagate along its axonal tree at a velocity $v(\mathbf{r}) \approx 10 \text{ m s}^{-1}$. This propagation can be described by damped wave equations for the fields ϕ_a [19]. After Fourier transforming in time, one finds, in terms of the incident signals,

$$D_a(\mathbf{r}, \omega) \phi_a(\mathbf{r}, \omega) = \sum_b J_{ab}(\mathbf{r}, \omega) \phi_b(\mathbf{r}, \omega), \quad (2)$$

where

$$D_a(\mathbf{r}, \omega) = [1 - i\omega/\gamma_a(\mathbf{r})]^2 - r_a^2 \nabla^2; \quad (3)$$

$$J_{ab}(\mathbf{r}, \omega) = L_{ab}(\mathbf{r}, \omega) G_{ab}(\mathbf{r}) e^{i\omega\tau_{ab}(\mathbf{r})}; \quad (4)$$

$\gamma_a(\mathbf{r}) = v(\mathbf{r})/r_a$ is a measure of the damping; r_a is the mean range of axons a ; the gain G_{ab} represents the scaled response strength in neurons a due to a unit signal incident from neurons of type b ; and τ_{ab} represents a pure delay—as in signal transmission between the cortex and the thalamus, for example—and appears as an exponent due to the temporal Fourier transform Using Eq. (2) and the connectivities shown in Fig. 2, the wave equation for excitatory cortical neurons follows as

$$D_e(\mathbf{r}, \omega) \phi_e(\mathbf{r}, \omega) = J_{ee}(\mathbf{r}, \omega) \phi_e(\mathbf{r}, \omega) + J_{ei}(\mathbf{r}, \omega) \phi_i(\mathbf{r}, \omega) + J_{es}(\mathbf{r}, \omega) \phi_s(\mathbf{r}, \omega). \quad (5)$$

The analogous equations for cortical inhibitory, specific relay, and reticular neurons can also be deduced from Eq. (2), and the quantities ϕ_i , ϕ_s , and ϕ_r can be eliminated to give the

transfer function of a stimulus ϕ_n to ϕ_e [10],

$$\begin{aligned} & \left([1 - J_{sr}(\mathbf{r}, \omega)J_{rs}(\mathbf{r}, \omega)] \{ [1 - J_{ei}(\mathbf{r}, \omega)] D_e(\mathbf{r}, \omega) - J_{ee}(\mathbf{r}, \omega) \} \right. \\ & \quad \left. - J_{es}(\mathbf{r}, \omega) [J_{se}(\mathbf{r}, \omega) + J_{sr}(\mathbf{r}, \omega)J_{re}(\mathbf{r}, \omega)] \right) \phi_e(\mathbf{r}, \omega) \\ & = J_{es}(\mathbf{r}, \omega) J_{sn}(\mathbf{r}, \omega) \phi_n(\mathbf{r}, \omega), \end{aligned} \quad (6)$$

of which the uniform case previously derived is a special case.

Measured large-scale cortical potentials are proportional to the mean cellular membrane currents, which are in turn proportional to the firing rates $\phi_{e,i}$. Cortical excitatory neurons generate most of the measurable potential on the scalp, because they are larger than inhibitory neurons and better aligned to generate observable signals [8,12]. In the present work, we ignore the effects of skull volume conduction, which are significant only for wave numbers $k \geq 15 \text{ m}^{-1}$ [7,20], and (via the dispersion relation) are significant only for correspondingly high frequencies ($\geq 25 \text{ Hz}$). At the alpha frequency, which is the primary interest of the present work, the power is little affected by the short-scale wave number filtering through the skull, and we are justified in ignoring skull conduction. Thus, in the absence of skull volume conduction, the power spectrum on the head is given by the squared modulus of the signal ϕ_e , to within a constant of proportionality.

B. Coupled mode equations

The multiple position-dependent parameters in Eq. (6) can be treated via coupled mode equations. We note that Eq. (6) is of the general form

$$A(\mathbf{r}, \omega) \phi_e(\mathbf{r}, \omega) = B(\mathbf{r}, \omega) \phi_n(\mathbf{r}, \omega). \quad (7)$$

Activity in this model is relatively insensitive to precise boundary conditions [6,17,18], so we investigate a simple cortical geometry in the first instance. Taking the Fourier transform in space, and applying rectangular periodic boundary conditions on a cortex of size $l_x \times l_y$, this becomes a discrete convolution

$$\sum_{\mathbf{K}} A(\mathbf{k} - \mathbf{K}, \omega) \phi_e(\mathbf{K}, \omega) = \sum_{\mathbf{K}} B(\mathbf{k} - \mathbf{K}, \omega) \phi_n(\mathbf{K}, \omega), \quad (8)$$

where \mathbf{k} and \mathbf{K} range over the values $\mathbf{k}_{mj}, \mathbf{K}_{mj} = (2\pi m/l_x, 2\pi j/l_y)$, and m and j are integers.

In previous work, the nonuniformity of a single parameter $t_0(\mathbf{r}) = 2\tau_{es}(\mathbf{r}) = 2\tau_{se}(\mathbf{r}) = 2\tau_{re}(\mathbf{r})$, which is the corticothalamic loop propagation delay, was addressed to investigate the phenomenon of alpha splitting [10]. Here, we vary multiple parameters simultaneously, and the analysis is not analytically tractable. We instead define the spatial variation of each parameter in the real domain separately. Nonuniformities of any functional form can be used, although the sinusoids which are the Fourier components of Eq. (8) are the natural choice in the present formalism. We then combine the spatial variations numerically in the real domain to calculate the functions A and B in Eq. (7). Care must be taken when handling the term ∇^2 since this cannot be transformed numerically. Instead, it must be isolated before Fourier transforming. Using Eq. (6) gives

$$A(\mathbf{r}, \omega) = \frac{(1 - i\omega/\gamma_e)^2}{r_e^2} - \nabla^2 - \frac{J_{ee}(1 - J_{sr}J_{rs})(J_{se} + J_{sr}J_{re})}{r_e^2(1 - J_{ei})(1 - J_{sr}J_{rs})}, \quad (9)$$

$$B(\mathbf{r}, \omega) = \frac{J_{es}J_{sn}}{r_e^2(1 - J_{ei})(1 - J_{sr}J_{rs})}. \quad (10)$$

The analytical Fourier transform k^2 of $-\nabla^2$ can then be added to the numerical transform of the remaining terms in Eq. (9), to produce the Fourier transform of A . The Fourier transform of B can be obtained numerically from Eq. (10). Thus we produce an equation of the form (8), which can be written as a matrix equation $\mathbf{A}\Phi_e = \mathbf{B}\Phi_n$, or $\Phi_e = \mathbf{A}^{-1}\mathbf{B}\Phi_n = \mathbf{M}\Phi_n$, where the size of each matrix depends on the number of modes M_{\max} retained after truncation [in one dimension, \mathbf{A} and \mathbf{B} are $(2M_{\max} + 1) \times (2M_{\max} + 1)$ matrices and Φ_e is a $(2M_{\max} + 1) \times 1$ column matrix] [10]. Note that A and B in Eq. (8) represent mode coupling between spatial nonuniformities; their diagonals represent coupling between same-order modes, and thus represent uniform activity. The term $-\nabla^2$ derives from the wave equation and is present regardless of the nonuniformities; its transform k^2 should thus only be added to the terms in Eq. (8) which govern spatially uniform activity. In the above formalism, these terms appear along the diagonal of the numerically transformed matrix \mathbf{A} .

We have shown previously [10] that the power spectrum at a given \mathbf{r} is given by

$$P(\mathbf{r}, \omega) = |\phi_n(\omega)|^2 \sum_{\mu, \nu} \exp[i(\mathbf{k}_\mu - \mathbf{k}_\nu) \cdot \mathbf{r}] (\mathbf{M}\mathbf{M}^\dagger)_{\mu\nu}, \quad (11)$$

for spatially white noise, where μ and ν label matrix elements. By averaging Eq. (11) over position, the mean power can be written

$$P(\omega) = |\phi_n(\omega)|^2 \text{Tr}(\mathbf{M}\mathbf{M}^\dagger), \quad (12)$$

where ϕ_n is independent of ω if the noise is also temporally white. In the present work, we restrict the nonuniformities to one dimension, since the most marked variations in alpha properties are from the front to the back of the head [1].

C. Stability

In this section we give a brief overview of stability in the model as it pertains to the present work. In previous work using the uniform model (i.e., with spatially uniform parameters) to analyze normal arousal states and epileptic seizures, we found that instability boundaries in parameter space approximately occur where [21]

$$0 = (1 - i\omega/\gamma_e)^2 - x - \frac{y(1 - G_{srs})}{1 - G_{srs}L^2} e^{i\omega t_0}, \quad (13)$$

$$x = G_{ee}/(1 - G_{ei}), \quad (14)$$

$$y = \frac{G_{ese} + G_{esre}}{(1 - G_{srs})(1 - G_{ei})}, \quad (15)$$

is satisfied, where for brevity we have written $G_{sr}G_{rs}$ as G_{srs} ; $G_{es}G_{se}$ as G_{ese} ; and, $G_{es}G_{sr}G_{re}$ as G_{esre} . The quantities x and

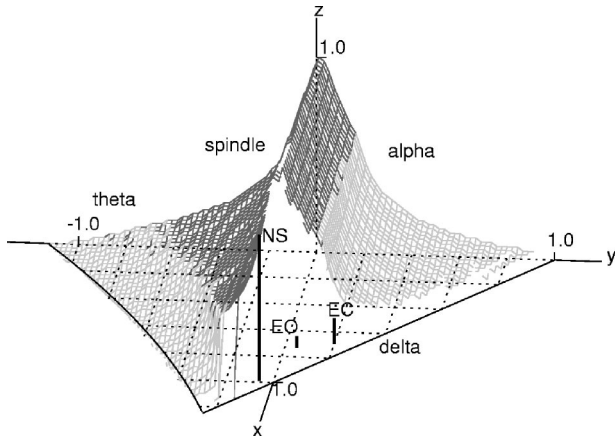


FIG. 3. Stability zone in xyz space. The surface is shaded according to instability type: the transparent front right face corresponds to a zero-frequency instability; the top right face corresponds to alpha-frequency (≈ 10 Hz) instability; the top central surface corresponds to a spindle-frequency (≈ 15 Hz) instability; and the top left face corresponds to a theta-frequency (≈ 3 Hz) instability. Approximate locations are shown of eyes-open (EO), eyes-closed (EC), and normal sleep (NS), with each state located at the top of its bar.

y relate to cortical and corticothalamic activity, respectively, and

$$z = -G_{srs}\alpha\beta/(\alpha + \beta)^2 \quad (16)$$

parametrizes intrathalamic activity; thus the system can be approximately parametrized in a reduced three-dimensional (xyz) space. The stability zone in xyz space defined by Eq. (13) is shown in Fig. 3. The alpha instability boundary is indicated on the upper right of the figure. Proximity to this boundary manifests itself in the spectrum as increased activity at the alpha frequency, since cortical activity approaches instability and hence the maximum firing rates typical of seizures. Indeed, if the boundary is crossed, the brain goes into a limit cycle near 10 Hz, which is possibly correlated to a seizure, via an instability of the alpha peak [21]. Also shown is the slow-wave boundary (the front unshaded surface), through which the brain passes into slow-wave (< 1 Hz) instability. This boundary follows the plane $x + y = 1$ [21], or

$$G_{ee} + G_{ei} + \frac{G_{ese} + G_{esre}}{1 - G_{srs}} = 1. \quad (17)$$

The spindle and theta boundaries are also indicated in Fig. 3, through which the brain passes into spindle (≈ 15 Hz), and ≈ 3 Hz spike-and-wave theta instabilities, respectively [21]. More generally, proximity to any instability boundary manifests itself as increased activity at the corresponding frequency.

The normal states of arousal lie within the stability zone in Fig. 3; the approximate locations of waking eyes closed (EC), waking eyes open (EO), and normal sleep (NS) are indicated in the zone. These approximate locations have been inferred by examination of typical spectra, extensive investi-

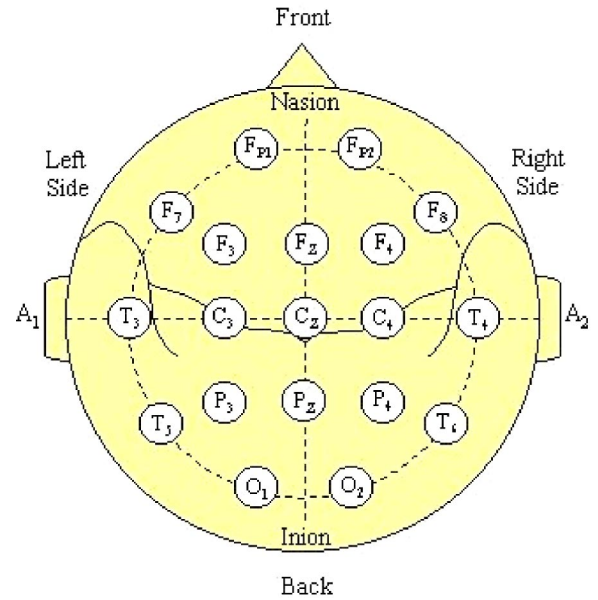


FIG. 4. Map of the head indicating some standard electrode sites. Some brain regions are also indicated: prefrontal (F_p), frontal (F), central (C), posterior (P), temporal (T), and occipital (O).

gation of the model, and comparisons with data from a wide variety of experiments. For a thorough discussion of the model parameters see Robinson *et al.* [20].

Note that the eyes-closed state lies closer to both the slow-wave and alpha instability boundaries than does the eyes-open state. In accordance with the above discussion, the eyes-closed state hence has larger peaks at low and alpha frequencies than the eyes-open state; i.e., it has more salient features than the eyes-open spectrum because of its relatively marginal stability. The stability of these states is discussed further in Sec. VI in light of the results of Sec. V.

III. PARAMETER NONUNIFORMITIES

In this section, we identify the effects on the power spectrum of introducing spatial nonuniformities into the model parameters; this initial investigation is exploratory, and will determine which parameters strongly affect the spectrum, and how. This will help us identify any parameters which need to be modeled by the full nonuniform model, and which frequencies are most strongly affected by nonuniformities, and hence need the full nonuniform model to be accurately studied. Actual nonuniformities in the brain are deduced in Sec. IV. We also compare the spectra generated by uniform and nonuniform parameter topographies, in order to determine the extent to which spatial nonuniformities in parameters affect the locally measured activity. That is, we examine the dependence of local spectra on activity elsewhere. This will determine the validity or otherwise of using the local effective value (LEV) model to infer precise spatial parameter variations.

We first illustrate a common reference map of the brain, shown in Fig. 4, on which several brain regions and common electrode sites are indicated. In the following, we use l_x

=0.8 m, the approximate circumference of the brain, which was determined by scaling the head circumference to account for cortical convolutions [22]. We take the front of the head to correspond to $d=0$ m, and the back to $d=0.4$ m. From Fig. 4 we see that this puts $d=0$ m in the prefrontal region, $d=0.2$ m in the central region, and $d=0.4$ m in the occipital region, where alpha power typically dominates [1].

A. Spectral effects

A nonuniformity is introduced into each model parameter separately to determine the way in which such nonuniformities affect the power spectrum at different locations across the head. In this subsection, we use the fully nonuniform model. We model the nonuniformity in a given parameter as a sinusoid; this is the natural choice, since it is the first Fourier component. In this exploratory investigation, the phase of the sinusoid is chosen arbitrarily. The nonuniformities introduced here are not intended to reflect actual nonuniformities in the brain; realistic nonuniformities are deduced in Sec. IV. We shall henceforth refer to the exploratory spectra in this section as illustrative, or theoretical spectra, to emphasize that they are not intended as predictions for actual spectra in the brain, but are instead a theoretical study of the effects of different types of parameter nonuniformity.

The effects on the illustrative theoretical local spectra of varying the parameters across the head are shown in Figs. 5 and 6. In each figure, the first column shows the (prefrontal) spectrum at $d=0$ m; the second column shows the (central) spectrum at $d=0.2$ m; and the third column shows the (occipital) spectrum at $d=0.4$ m. In Fig. 5, each row corresponds to a different gain parameter, as labeled: $G_{ee}, G_{ei}, G_{ese}, G_{esre}, G_{srs}$ and $G_{sn}\phi_n$. In Fig. 6, each row also corresponds to a different parameter: the dendritic rate constant α , the damping γ_e , and the corticothalamic delay t_0 . All parameters other than the one under investigation are held constant at their nominal (global) values, which have been estimated by extensive modeling and comparisons with physiology and anatomy [20]. In each case, the parameter under investigation is varied sinusoidally over half a period from front to back, with maximum magnitude at the front ($d=0$ m), and minimum magnitude at the back ($d=0.4$ m). The solid line represents the local LEV spectrum when no parameters are varied; it is the same in each of the panels. The dotted line represents the case of a sinusoidal variation with amplitude equal to 10% of the parameter's nominal value, and the dashed line corresponds to a variation with an amplitude of 20% of the nominal value.

Let us consider first the gain parameters in Fig. 5, which uses a log-log scale so that effects at frequencies below 1 Hz can be identified. Row (a) shows the effect of varying G_{ee} , the dimensionless gain reflecting the connection numbers and strengths due to cortical excitatory neurons. At and below the alpha frequency, the spectral power is increased where G_{ee} has a maximum (prefrontally here); the inverse is true where G_{ee} has a minimum (occipitally here). Row (b) of Fig. 5 shows the effect of varying G_{ei} , the dimensionless gain reflecting the connection numbers and strengths between cortical excitatory and inhibitory neurons. We see that where the

magnitude of this negative gain is greatest (prefrontally here), the power at both low and alpha frequencies is the smallest, and vice versa (occipitally here). We can understand this effect in two ways: first, using the insights from the model, we note that decreasing G_{ei} , or increasing G_{ee} , increases the cortical state parameter x defined in Sec. II A, and hence moves that local region of the brain closer to both the slow-wave and alpha instability boundaries. This manifests itself in the theoretical spectrum as increased activity at both slow-wave and alpha frequencies as cortical activity approaches instability, as discussed in Sec. II A. Second, in terms of physiology, we can infer that a decrease in negative cortical activity would lead to an increase in measurable voltage, since the inhibitory neurons are having a decreased inhibitory effect on their excitatory counterparts. Similarly, an increase in positive cortical activity would lead to an increase in measurable voltage.

Row (c) in Fig. 5 shows the effect on the illustrative spectrum of varying $G_{ese}=G_{es}G_{se}$, the strength of the direct, positive corticothalamic feedback loop that does not pass through the reticular nucleus, shown in Fig. 2. In this case, where G_{ese} is small (occipitally here), there is lower power at low and alpha frequencies. Again, we can explain this using the stability discussion: decreasing G_{ese} decreases the corticothalamic state parameter y , taking the local region of the brain further from the instability boundary and hence to lower activity. The converse is true when G_{ese} is increased (prefrontally here). Intuitively, we can understand that decreasing the positive feedback G_{ese} will decrease cortical activity, and vice versa. This effect is noticeable at the alpha frequency, because resonance in the corticothalamic loop is the alpha mechanism in our model. Indeed, the corticothalamic delay $t_0 \approx 85$ ms is the dominant contributor to the alpha frequency, which is given by [10]

$$f_\alpha(\mathbf{r}) \approx [t_0(\mathbf{r}) + 1/\alpha(\mathbf{r}) + 1/\beta(\mathbf{r})]^{-1}. \quad (18)$$

Rows (d) and (e) of Fig. 5 show that power at low frequencies is lowest at maximums of $|G_{esre}|=|G_{es}G_{sr}G_{re}|$ and $|G_{srs}|=|G_{sr}G_{rs}|$, respectively (i.e., prefrontally here); however, the effects are very slight. The theoretical spectrum elsewhere is largely unaffected by the nonuniformities in these parameters. Row (f) of Fig. 5, however, indicates that the spectrum is affected at all frequencies by nonuniformities in $G_{sn}\phi_n$, which represents the strength of subthalamic inputs into the thalamus, as shown in Fig. 2. Where subthalamic input is larger than the average value (prefrontally here), the power at all frequencies is also larger than elsewhere; where the input is smaller (occipitally here), the power is decreased. This effect is independent of frequency, since the input signal is temporally white in our model. Thus spatial nonuniformities in $G_{sn}\phi_n$ scale the power nonuniformly across the brain; nonuniformities in $G_{sn}\phi_n$ can thus incorporate effects such as variations in volume conduction through the skull, which similarly scale the recorded power [12].

Let us now consider the effects of varying the temporal parameters, as seen in Fig. 6. These plots are shown on a log-linear scale to emphasize the illustrative spectra around the alpha frequency; the theoretical spectra below 1 Hz are unaffected by the nonuniformities in these parameters. Row

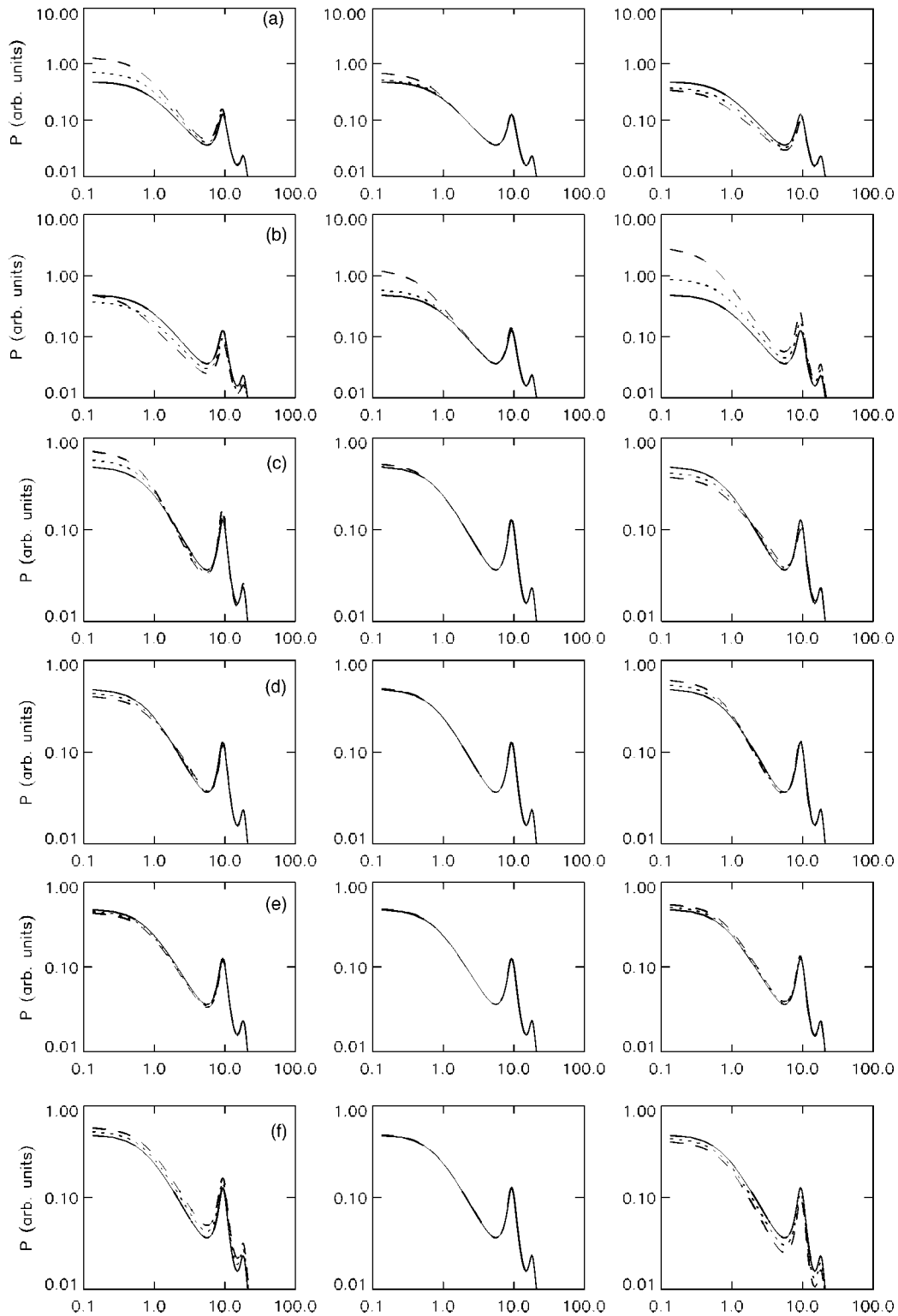


FIG. 5. Investigation of the effects on the spectrum of spatial nonuniformities in the gain parameters, on log-log axes. Each parameter is varied sinusoidally over half a period from front to back, with maximum magnitude at the front. The first column corresponds to the front of the head ($d=0$ m), the second column corresponds to the middle of the head ($d=0.2$ m), and the third column corresponds to the back of the head ($d=0.4$ m). The solid line represents the local spectrum when no parameters are varied; it is the same in each of the panels. The dotted line corresponds to a variation with amplitude of 10% of the parameter's nominal value, and the dashed line corresponds to a variation amplitude of 20% of its nominal value. All parameters other than the one under investigation are held constant at their nominal values. Row (a) involves variations in G_{ee} ; row (b) involves variations in G_{ei} ; row (c) involves variations in G_{ese} ; row (d) involves variations in G_{esre} ; row (e) involves variations in G_{srs} ; and row (f) involves variations in $G_{sn}\phi_n$.

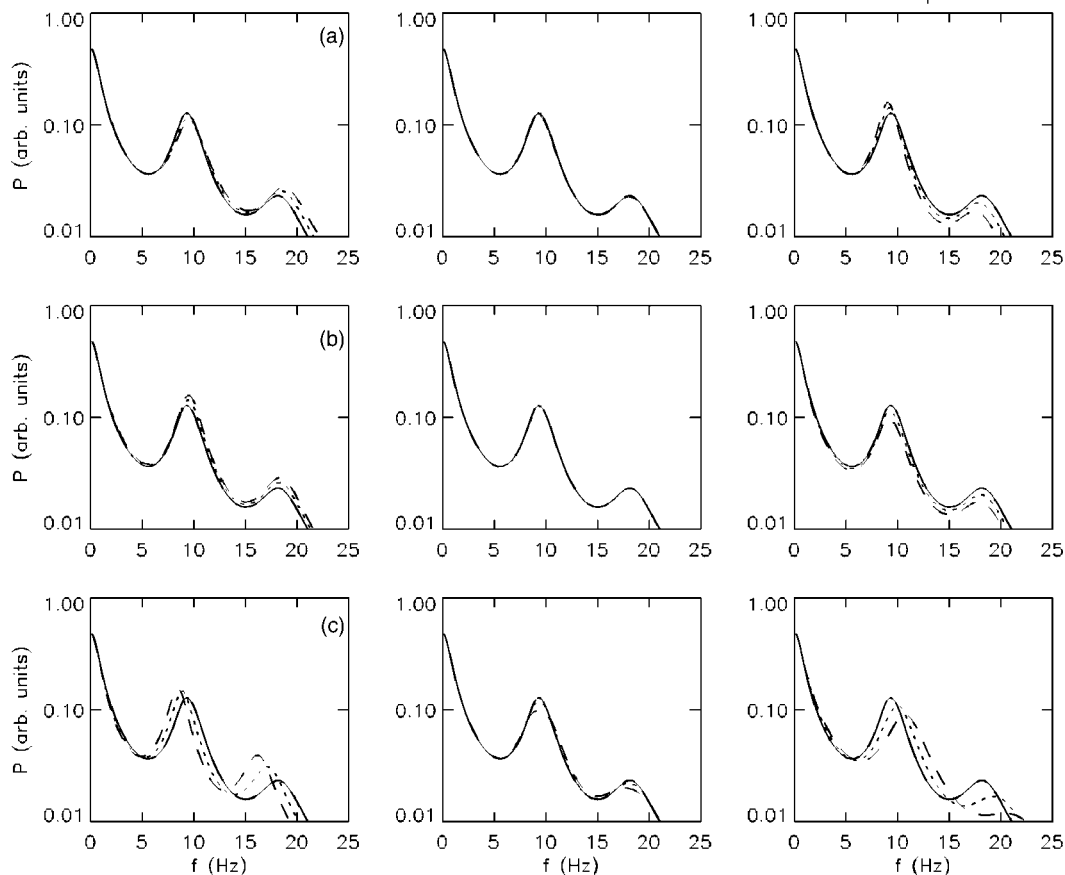


FIG. 6. Investigation of the effects on the spectrum of spatial nonuniformities in the temporal model parameters, on log-linear axes. Each parameter is varied sinusoidally over half a period from front to back, with maximum magnitude at the front. The first column corresponds to the front of the head ($d=0$ m), the second column corresponds to the middle of the head ($d=0.2$ m), and the third column corresponds to the back of the head ($d=0.4$ m). The solid line represents the local spectrum when no parameters are varied; it is the same in each of the panels. The dotted line corresponds to a variation with amplitude of 10% of the parameter's nominal value, and the dashed line corresponds to a variation amplitude of 20% of its nominal value. All parameters other than the one under investigation are held constant at their nominal values, except $\beta=4\alpha$. Row (a) involves variations in α ; row (b) involves variations in γ_e ; and row (c) involves variations in t_0 .

(a) of Fig. 6 shows the effect of spatial nonuniformities in the dendritic rate constant α , with $\beta=4\alpha$. Decreasing α , and hence β , increases the alpha peak amplitude. At higher frequencies, the local background spectrum is steeper where α is low, because the low-pass cutoff in the frequency filter given by Eq. (1) is correspondingly reduced. The state parameters x , y , and z are unaffected by changes in α ; however, decreasing α moves the alpha instability boundary itself, via its influence on the dendritic filter function L , as seen for example in Eq. (13). Thus the increase in alpha activity where α is low, is due to proximity to the alpha instability boundary, discussed in Sec. II A. There is also a shift in the alpha frequency as a result of the nonuniformities in α : where α is smaller than its mean value (occipitally here), the alpha peak is shifted to lower frequency; decreased α corresponds to increased dendritic delays in the corticothalamic loop, and hence an increase in the total loop delay, which leads to a decrease in the alpha frequency, as summarized in Eq. (18).

Row (b) of Fig. 6 shows the theoretical local spectra when only the damping rate γ_e is varied. Where the damping rate is low (occipitally here), activity at and above the alpha fre-

quency is decreased, in agreement with previous findings that at high frequencies the power is proportional to γ_e [3]. This intuitively paradoxical result can be explained by referring to the stability discussion in Sec. II A: although γ_e does not affect x , y , or z , it moves the alpha instability boundary itself, as can be seen from Eq. (13). Thus decreasing γ_e moves the boundary outward, which effectively leaves the brain further from the boundary, and hence with less activity.

Row (c) of Fig. 6 shows the effect on the illustrative, theoretical local spectrum of varying the corticothalamic loop propagation delay, t_0 . The greatest effect is the change in alpha frequency: where the loop delay is smallest, the alpha frequency is highest, as expected from Eq. (18). The alpha peak power is also sensitive to nonuniformities in t_0 : where t_0 is decreased, the power is also decreased, and vice versa. Note that this effect was not investigated during previous work on nonuniformities in t_0 [10], which only investigated frequency effects. Indeed, the previous work proposed that the corticothalamic delay is smaller at the back of the head than at the front [10], which is consistent with the frequency shift in row (c); however, the reduction in power which is apparent in the occipital frame of row (c) implies

that nonuniformities in this quantity alone cannot account for the simultaneously observed occipital increase in the alpha peak power.

From this illustrative study, we find that none of the parameters whose nonuniformities strongly affect activity near the alpha frequency do so exclusively. The parameters that strongly affect alpha activity are G_{ei} , G_{ese} , γ_e , α , and t_0 ; these all affect activity at other frequencies too. However, observed EEG spectra indicate that front-to-back variations in activity are not significant below the alpha frequency [2,23,24]; it is therefore unlikely that a single parameter will account for the observed site dependence of EEG spectra. Indeed, parameters, which from physiological arguments are likely to vary together, often have competing and hence balancing effects; for example, the principle of random connectivity, whereby the number of interconnections between neural types are assumed to be proportional to the number of available synapses, implies that G_{ee} and $|G_{ei}|$ are likely to vary together. Row (b) in Fig. 5 shows that decreasing the gain $|G_{ei}|$ not only increases alpha power, but also has a large positive effect at very low frequencies. Decreasing the gain G_{ee} [row (a)] has a large negative effect at very low frequencies. Thus their competing influences at low frequencies would tend to balance, thereby helping to preserve cortical stability, from Eq. (14). Similarly, the fact that the thalamic gains G_{ese} , G_{esre} , and G_{srs} depend on shared anatomical structures, implies that these gains are likely to have correlated spatial profiles. Rows (c)–(e) in Fig. 5 shows that these gains have competing effects at low frequencies. Thus, if they indeed vary together, their compensating influences at low frequencies will tend to balance, thereby ensuring cortical stability, from Eq. (17).

B. Local independence

We now turn our attention to determining the extent to which spatial nonuniformities in the model parameters affect the locally measured activity. Specifically, we investigate the extent to which the locally measured spectrum, which arises from nonuniform parameter profiles, can be approximated by the spectrum of the local effective value (LEV) model; we term this the local independence approximation. In this section, we test the local independence approximation by comparing spectra generated from the LEV model with spectra generated from the nonuniform one. Recall that the central columns of Figs. 5 and 6 show both the LEV spectrum (solid line) and the nonuniform spectrum at $d=0.2$ m. For each parameter, the spectra localized at the center of the head are very similar to the corresponding LEV spectra. This may be due to the sinusoidal parameter variations, which are zero at this point. Mode coupling effects ensure, however, that the nonzero variation at other points contribute to slight effects here, which are too small to be seen for most parameters; however, such effects can be easily seen at low frequencies in the central columns of rows (a) and (b) in Fig. 5 for variations in G_{ee} and G_{ei} , respectively, and at the alpha and beta resonances in the central column of row (c) in Fig. 6, for variations in t_0 . We investigate these effects more thoroughly below.

The above results imply that the local independence approximation in the LEV model is reasonable for most parameters, at least where the nonuniformity is symmetrical about the point of comparison. In order to test the more general case, we compare LEV and nonuniform spectra in Fig. 7, where the nonuniformity is not symmetrical about the point of comparison. The nominal parameter values are the same as those used in Figs. 5 and 6. In each case, all parameters, other than the one under investigation, are held constant at their nominal values for both the LEV and nonuniform spectra. For the parameter under investigation, the nonuniform spectrum is calculated at the front of the head ($d=0$ m), while the parameter is varied sinusoidally across the head over half a period, with maximum magnitude at the front of the head. The amplitude of the variation is 20% of the parameter's nominal value. The LEV spectrum is calculated using 120% of the parameter's nominal value, so that all the parameters have the same values at $d=0$ m for both the LEV and nonuniform spectra. Note that the LEV spectrum is therefore different for each parameter investigated. The solid lines in Fig. 7 show the LEV spectra. The dotted lines show the corresponding nonuniform spectra. Each panel in Fig. 7 shows the spectra measured at the front of the head when a different parameter is varied: respectively, G_{ee} , G_{ei} , G_{ese} , G_{esre} , G_{srs} , $G_{sn}\phi_n$, α , γ_e , and t_0 .

The solid line in Fig. 7(a) shows the spectrum generated from uniform parameter profiles, with all parameters at their frontal values. The dotted line shows the spectrum generated at the front of the head, when G_{ee} decreases sinusoidally to a minimum at the back of the head; all other parameters are uniform at their frontal values. We see a significant decrease in the nonuniform spectrum compared to the LEV one, at low frequencies, as well as a slight difference at the alpha frequency. By comparison with row (a) of Fig. 5, we see that a decrease at low frequencies is associated with a decrease in the magnitude of G_{ee} . That is, the lower G_{ee} elsewhere in the cortex reduces its effective value at $d=0$ m. We use the term “effective” value to mean the LEV value which would produce the most similar possible spectrum. The effect is only apparent at frequencies $f \lesssim 2$ Hz. We explain this by noting that the spatial nonuniformities are at a scale comparable to the size of the head. They therefore affect activity only at low wave numbers and hence, via the dispersion relation, only at low frequencies. Regarding the effect at the alpha frequency, we note that the alpha peak is due to weakly damped corticothalamic activity; the weak damping, and hence lower k , at this frequency enables activity at distant cortical sites to more easily propagate across the cortex and affect the locally-measured activity.

Figure 7(b) shows the effect on local independence of nonuniformities in G_{ei} . Again, there is a significant difference between the LEV (solid line) and nonuniform (dotted line) spectra at low frequencies, as well as a difference at the alpha frequency. By comparison with row (b) of Fig. 5, we see that the relative increase in the nonuniform spectrum is associated with a decrease in the magnitude of G_{ei} . That is, similarly to the above, the lower G_{ei} magnitude elsewhere in the cortex reduces its effective LEV magnitude frontally.

Similar effects are found in Figs. 7(c)–7(f), for G_{ese} , G_{esre} , G_{srs} , and $G_{sn}\phi_n$, respectively. That is, we see differences be-

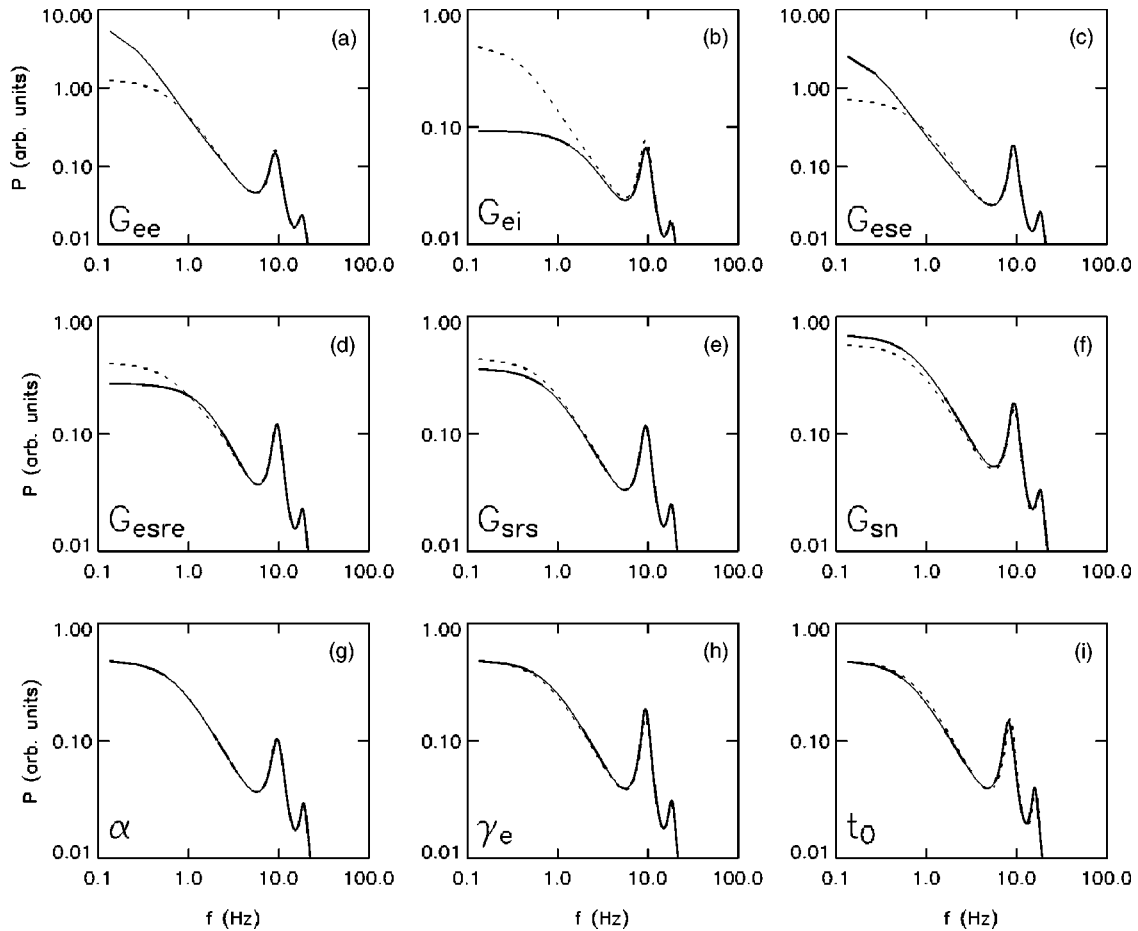


FIG. 7. Investigation of the extent to which local dynamics are affected by spatial nonuniformities in the model parameters. The solid line represents the uniform spectrum at the front of the head ($d=0$ m), and the dotted line represents the nonuniform spectrum at the front of the head when one parameter is varied. Each parameter is varied sinusoidally over half a period from front to back, with maximum magnitude at the front, and all parameters other than the one under investigation are held constant at their frontal values. Panel (a) tests nonuniformities in G_{ee} ; panel (b) tests nonuniformities in G_{ei} ; (c) tests G_{ese} ; (d) tests G_{esre} ; (e) tests G_{srs} ; (f) tests $G_{sn}\phi_n$; (g) tests α ; (h) tests γ_e ; and (i) tests nonuniformities in t_0 .

tween the LEV and nonuniform spectra at low frequencies, as well as slight differences at the alpha frequency for G_{ese} and $G_{sn}\phi_n$. Comparing the direction of the difference with the occipital column in Fig. 5, we deduce that, for each of these gain parameters, the lower magnitude elsewhere in the cortex reduces its effective LEV frontal magnitude.

Figures 7(g)–7(i) show the effects of nonuniformities in α , γ_e and t_0 , respectively; there is little difference between the LEV and nonuniform spectra. This is in agreement with the above, since spatial variations in these parameters only weakly affect the spectrum below ≈ 2 Hz, as seen in Fig. 6. In panels (h) and (i), however, there is a slight effect at the alpha frequency due to the weaker damping here.

In conclusion, we have demonstrated that for an eyes-closed state, local activity is largely independent of activity elsewhere on the cortex. There are two major exceptions, due to the propagation of large-scale activity: below ≈ 2 Hz, the local dynamics are dependent on low-wave-number activity at distant sites as reflected in the dispersion relation; and, at the alpha frequency, the weaker damping enables efficient propagation of distant low- k activity, which thus affects local activity. The effect at the alpha frequency is less than that at

low frequencies. In these cases, spatial nonuniformities in the parameters should not be ignored. However, at most frequencies, locally measured activity can be assumed to be independent of spatial nonuniformities in the parameters, to a first approximation. These results were deduced using a low-order spatial eigenmode. Higher-order spatial eigenmodes are discussed in the following subsection.

C. Local vs global uniform spectra

We now investigate the extent of the improvement, or otherwise, which results from approximating the fully non-uniform spectrum by the local uniform (LEV) spectrum, rather than the global uniform one.

Figures 8(a) and 8(b) show the spectrum at the front of the head when all the parameters are spatially varied simultaneously, on log and linear scales respectively. As in Figs. 5–7, the parameters are varied sinusoidally over half a period, with maximum magnitude at the front of the head, and an amplitude of 10% of the parameter's nominal value. In both panels, the dotted line represents the global uniform spectrum, generated using the mean parameters; this spec-

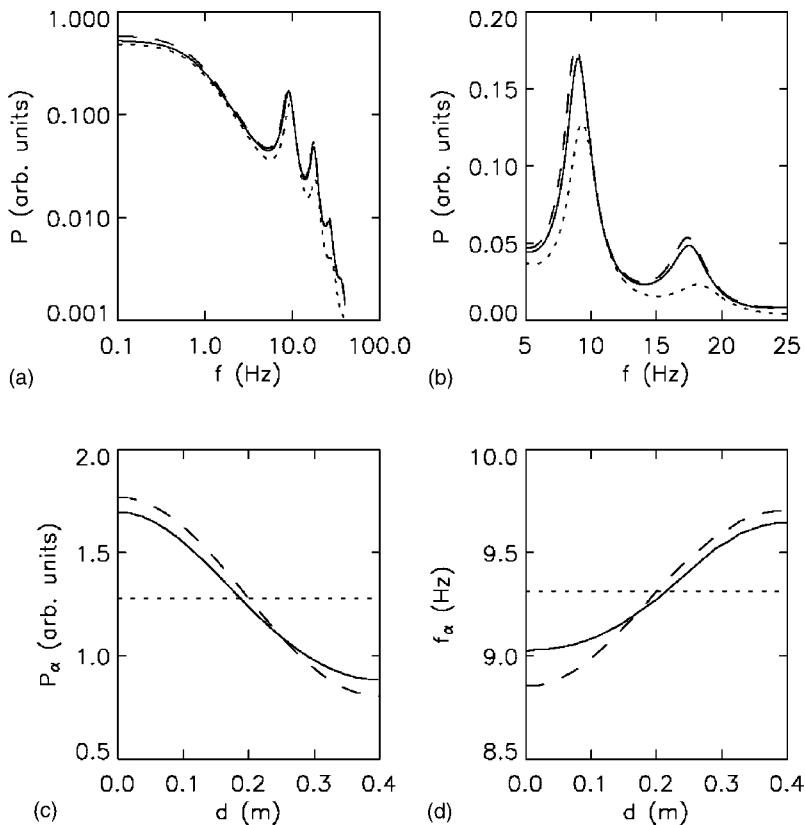


FIG. 8. Investigation of a case where all model parameters are varied simultaneously over half a sinusoid period, with maximum magnitude at the front of the head, and an amplitude of 10% of the parameter's nominal value. Panels (a) and (b) show the spectra at the front of the head, on log and linear scales, respectively. Panels (c) and (d) represent the power at the alpha peak and the frequency of the alpha peak, respectively, as a function of distance across the head. In each panel, the dotted line represents results from the global uniform model, the dashed line represents results from the LEV model, and the solid line represents results from the full nonuniform model.

trum does not vary across the head. The dashed line represents the LEV spectrum, generated from the uniform version of the model, using the local values. The solid line represents the spectrum generated using the nonuniform model. Much of the discrepancy between the two spectra has disappeared, especially at low frequencies; this is because the parameters are all being varied at once, and the competing effects seen in Fig. 7 at low frequencies cancel. Panels (a) and (b) show that at the front of the head for this parameter profile, the nonuniform spectrum lies between the local and global spectra; this is true across the whole head, and for other spatial profiles. This effect is due to the fact that the nonuniform spectrum at a local point tends towards the mean spectrum, because of dispersion effects from neighboring regions.

Figures 8(a) and 8(b) show only the spectrum at the front of the head, and indicate that at this point the LEV spectrum is a better approximation to the fully nonuniform spectrum, than is the global uniform spectrum; that is, the dashed line lies closer than the dotted line to the solid one. Two measures of the goodness of the approximation across the whole head are shown in panels (c) and (d), which indicate, as a function of distance across the head, the power at the alpha peak and the frequency of the alpha peak, respectively. These measures indicate that the LEV (dashed line) is a better approximation to the fully nonuniform spectrum (solid line) across the whole head, than is the global uniform spectrum (dotted line). Note that the global and LEV spectra coincide where the local parameters equal the mean parameters, which for the symmetrical parameter profile here occurs at $d=0.2$ m; note that at this point the actual, nonuniform spectrum is not coincident with the two uniform spectra.

For lowest-order sinusoidal parameter nonuniformities, the above arguments indicate that the LEV spectrum is a fair

approximation to the fully nonuniform spectrum. As the order of the nonuniformities increases, i.e., for higher-order spatial eigenmodes, the match between the nonuniform and LEV spectra becomes increasingly bad. For the nonuniformities in Fig. 8, the wavelength of the sinusoidal nonuniformity is $\lambda \approx 9r_e$, and the match is good. We investigated nonuniformities of various wavelengths, and found that for $\lambda \leq (4-5)r_e$, the match is no longer better than that provided by the global uniform spectrum. For such nonuniformities, the high- k oscillations imply that at a given location the local approximation is no longer valid, due to the effects of dispersion from neighboring points with very different parameter values. Note that this is an additional effect to head volume conduction in the skull, which also smears high- k activity.

Thus, for low-order nonuniformities, the LEV model captures the spatial dependence of the spectrum to a good first approximation. It remains to determine whether the nonuniformities in the brain are indeed of low order, and to determine their likely profiles. Those represented in Fig. 8 are clearly not the actual parameter nonuniformities, since the power at the alpha peak in this figure decreases towards the back of the head, contrary to observations [1]. In the following section, we aim to determine likely parameter nonuniformities by comparison with EEG data.

IV. INVERSE MODELING

Having investigated the effects of parameter nonuniformities in the model, we now aim to establish realistic bounds on these nonuniformities. We then apply these constraints in Sec. V to determine whether they can account for the ob-

served spectral dependence on position. Note that the discussion in this section is concerned with constraining the spatial variation in the parameters, not the mean values of the parameters *per se*; constraints on the parameters themselves are discussed extensively elsewhere [20].

EEG recordings of healthy adult subjects from the general community were obtained in a previous study [25] with the appropriate ethical clearances and informed consent, including consent for further analysis of the data, as in the present work. Subjects were 49 females and 51 males with a mean age of 44 years [standard deviation (SD) =16 years] and 45 years (SD=15 years), respectively. An electrode cap using the international 10–20 system of scalp sites was used to acquire the EEG data. EEGs were recorded at a 250-Hz sampling rate through a SynAmps™ amplifier using a linked ear-lobe reference and a low-pass third order Butterworth filter with –6 dB point at 50 Hz. Ocular artefacts were corrected offline according to the method of Gratton *et al.* [26]. For each EEG recording, the mean experimental power spectrum from 0–50 Hz was calculated for 27 successive 4-sec epochs.

We investigate likely front-to-back parameter trends by examining experimental data recorded from the normal subjects at five electrodes: F_{P1} , Fz, Cz, Pz, and O_2 , shown in Fig. 4. These electrodes were chosen because they lie in a straight line almost along the midline (prefrontal and occipital midline sites, E_{Pz} and O_z , were not available to us). The uniform LEV version of the model was fitted to the spectrum for each subject at each site, using an inverse-modeling routine in which the error between the experimental spectrum and the model spectrum was iteratively reduced using Levenberg-Marquardt nonlinear least-squares optimization [27,28]. Note that this is distinct from fitting the generalized nonuniform model described in Sec. II A, because the LEV model does not allow for mode coupling; the electrodes are fitted independently at each site. However, the results of the previous section indicate that this is adequate to a first approximation, and is very good for frequencies above 2 Hz. Two of the 100 subjects were excluded from the present study because the model could not be fitted to their spectra with sufficiently small χ^2 at all sites.

The results of the inverse-modeling are shown as solid circles in Figs. 9 and 10 as a function of distance across the head, where we take $d=0$ m to be the front of the head, and $d=0.4$ m to be the back of the head, as previously. Error bars correspond to one standard error of the mean (SEM). For each parameter, the mean value is also shown, as a dashed line, demonstrating that the parameters have significant nonuniformities.

In order to model the spatial nonuniformities in the parameters, note that, from the modal analysis in Sec. II A, the one-dimensional spatial dependence of a parameter p can be written in terms of its Fourier components as

$$p(x) = \sum_m p_m e^{ik_m x}, \quad (19)$$

where $k_m = 2\pi m/l_x$, and here $l_x = 0.8$ m. In general, the coefficients p_m are complex; however, in the present work we use real $p_m = p_{-m}$, since the use of complex values merely shifts

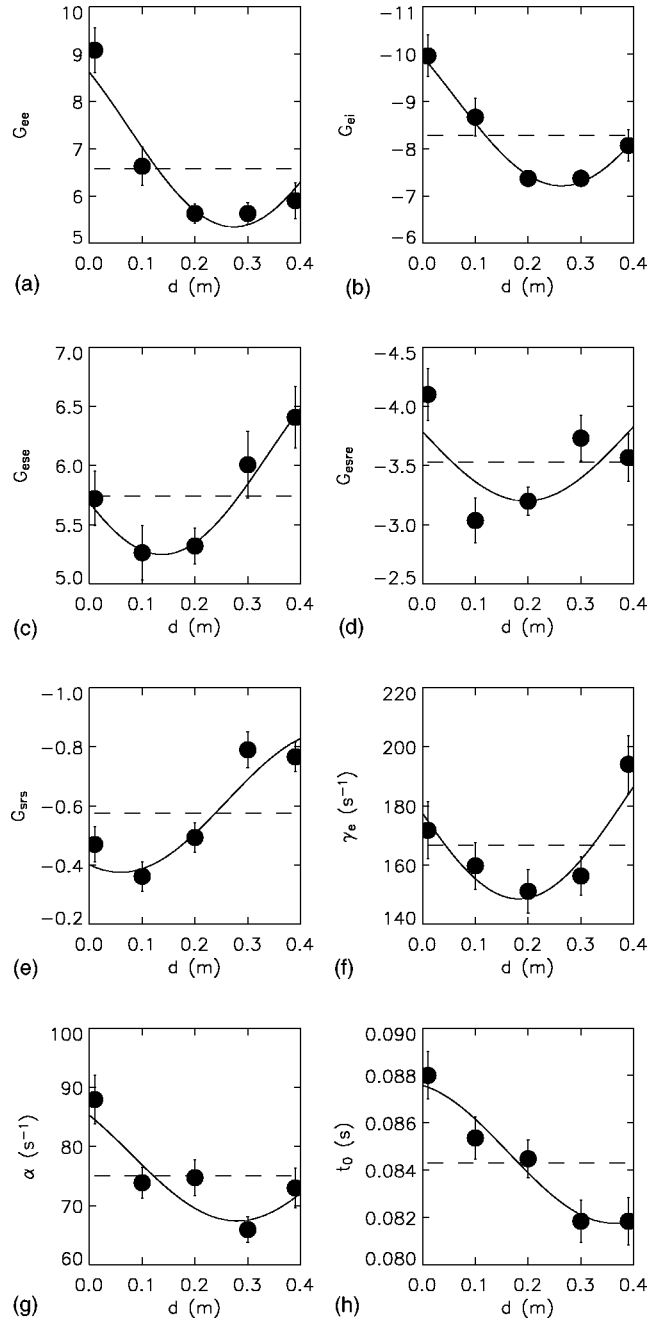


FIG. 9. Midline nonuniformities in the independent model parameters. Filled circles correspond to the data obtained from fitting the model to spectra recorded from 98 normal subjects; the mean is shown as a dashed line. Error bars correspond to one SEM, indicating that a good model should pass through at least 68% of them. The solid line shows the sinusoid of best fit, found using an iterative nonlinear least-squares χ^2 minimization fitting routine. Panel (a) shows the spatial nonuniformity in G_{ee} ; (b) shows the spatial nonuniformity in G_{ei} ; (c) shows the nonuniformity in G_{ese} ; (d) shows the nonuniformity in G_{esre} ; (e) shows the nonuniformity in G_{srs} ; (f) shows the nonuniformity in γ_e ; (g) shows the nonuniformity in α ; and (h) shows the spatial nonuniformity in t_0 .

$p(x)$ along the x axis and we have assumed periodic boundary conditions. To model the parameters, we retained only the three lowest order modes ($0, \pm 1$), giving

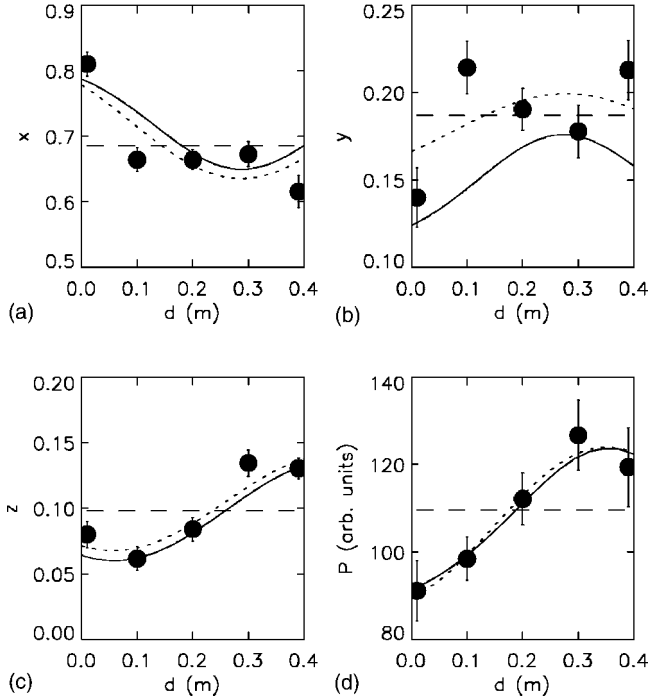


FIG. 10. Nonuniformities in the dependent model parameters. Filled circles correspond to the data obtained from fitting the model to spectra recorded from 98 normal subjects; the mean is shown as a dashed line. Error bars correspond to one SEM. The dotted lines show the sinusoids of best fit to the data, found using an iterative nonlinear least-squares χ^2 minimization fitting routine. The solid lines show the spatial profiles which arise in these dependent parameters, as a results of introducing the nonuniformities shown in Fig. 9 into the independent parameters. Panel (a) shows the cortical state parameter x ; (b) shows the corticothalamic state parameter y ; (c) shows the intrathalamic state parameter z ; and (d) shows the total power P . Note that the scales on the ordinate do not start at zero in all panels.

$$p(x) = a + b \sin\left(\frac{2\pi x}{l_x} + c\right), \quad (20)$$

where the phase parameter c accounts for shifting along the x axis. Thus the three coefficients, a , b , and c , represent the mean, amplitude, and phase of the sinusoid. For each parameter, we fitted a sinusoid of the form (20) to the data in Fig. 9. The coefficients were optimized using an iterative

gradient-expansion algorithm to compute a nonlinear least squares fit in order to minimize the χ^2 error statistic [27]; the best-fit coefficients are shown in Table I. Note that the coefficient a represents the mean of the sinusoid, not the mean of the data, and as such is different to previously estimated mean parameter values [28]. The goodness of fit was estimated by calculating the incomplete gamma function,

$$Q(\chi^2|\nu) = \frac{\int_0^{\chi^2} e^{-t} t^{\nu/2-1} dt}{\int_0^{\infty} e^{-t} t^{\nu/2-1} dt}, \quad (21)$$

where ν represents the number of degrees of freedom of the fit, and is found by subtracting the number of fitted coefficients from the number of data points being fitted, giving $\nu = 2m$ in the present case. The quantity Q is the probability that a value of χ^2 as poor as the value calculated should occur by chance if the fit is correct. If Q is larger than ≈ 0.1 , the goodness-of-fit is believable [27], and if Q is smaller than ≈ 0.001 , the model should be rejected. Between these two extremes, the model may still be correct if the errors in the data are nonnormal or underestimated. For each of the model parameters in Fig. 9, $Q \geq 0.08$, thus a sinusoid of period l_x is likely to accurately model the spatial nonuniformities in all the parameters. The Q values are shown in Table I. We can thus capture the spatial variations in the model parameters by using the lowest-mode sinusoids, with varying mean, amplitude, and phase.

The nonuniformities in the dependent state parameters x , y , and z were investigated in three ways. Recall that these parameters represent cortical, corticothalamic, and thalamic activity, respectively, in the reduced three-dimensional parametrization; they are given by Eqs. (14)–(16). First, the LEV model was fitted to the experimental spectra recorded from 98 subjects at each electrode, as above. The results are shown as filled circles in Fig. 10, with error bars corresponding to one SEM. The means of the data are shown as dashed horizontal lines, demonstrating that these parameters also have significant spatial nonuniformities. Second, sinusoids of best fit were found using the least-squares optimization method outlined above. These sinusoids of best fit are plotted in Fig. 10 as dotted lines. Third, the parameters x , y , and z were calculated from Eqs. (14)–(16), respectively, using the nonuniform model and the nonuniformities in the indepen-

TABLE I. The best-fit coefficients a , b , and c , when a sinusoid of the form $y = a + b \sin(2\pi x/l_x + c)$, $l_x = 0.8$, was fitted to the spatial data from the $n=98$ subjects, using a nonlinear least-squares fitting routine. Also shown is the goodness-of-fit parameter Q , from Eq. (21), where $Q > 0.1$ indicates a good fit. The value of Q could not be obtained for $G_{sn}\phi_n$, since this quantity was not fitted directly to the data from the $n=98$ subjects.

	G_{ee}	G_{ei}	G_{ese}	G_{esre}	G_{srs}	$G_{sn}\phi_n$	γ_e	α	t_0
a	7.5	-9.1	6.1	-3.8	-0.61	1.1	180 s ⁻¹	79 s ⁻¹	0.085 s
b	-2.1	1.8	0.84	0.61	-0.22	0.14	-33 s ⁻¹	11 s ⁻¹	0.0030 s
c (rad)	5.7	5.7	3.6	0.04	4.2	5.2	0.13	2.5	1.9
Q	0.35	0.29	0.89	0.08	0.24	N/A	0.60	0.26	0.67

dent state parameters, indicated by the solid lines in Fig. 9. In each of x, y , and z , the two sinusoids have approximately the same amplitude and phase, and also have similar means except for y , where the sinusoids are slightly offset. [Note that in Figs. 10(a) and 10(b) the scales on the ordinates do not begin at zero.] The differences between the two curves arise from the fact that the results of the direct fits to x, y , and z (dotted lines) implicitly contain all convolutions between the terms in Eqs. (14)–(16), whereas the trends calculated from Eqs. (14)–(16) (solid lines) contain only the same-order terms; for example, the +1 mode for x is calculated only from the +1 modes in G_{ee} and G_{ei} , and contributions from coupling of the $+m$ and $1-m$ modes are ignored, for any integer m .

Although the fitted (dotted line) and calculated (solid line) nonuniformities are similar for x and y , in Figs. 10(a) and 10(b), they do not fit the data well (solid circles). This discrepancy perhaps arises because sinusoids of fixed period are not sufficient to accurately model the nonuniformities. However, x depends on G_{ee} and G_{ei} , and the sinusoidal fits to these parameters were good, from Table I. In any case, the nonuniform fit to the data is certainly an improvement on the uniform fit (dashed line). The parameter y depends in part on G_{esre} , which from Table I is a relatively poor fit, which may explain the greater discrepancy between the data and the deduced nonuniformities in Fig. 10(b). Generally, however, the nonuniform fits to both the independent (Fig. 9) and dependent (Fig. 10) parameters are a significant improvement on the uniform ones.

Consider now the total power, shown in Fig. 10(d). In this case the best fit and the modeled trend are almost coincident. This results from the fact that we were free to choose the coefficients of the sinusoid for the nonuniformity in $G_{sn}\phi_n$, since this quantity is the only parameter in which nonuniformities were not directly constrained by inverse modeling of the $n=98$ subjects. Recall that $G_{sn}\phi_n$ models subthalamic input, as well as changes in measured signal amplitude via volume conduction through the head. Thus its nonuniformities reflect nonuniformities in subthalamic input, and volume conduction, which may be due, for example, to spatial variations in skull thickness. The composite $G_{sn}\phi_n$ affects only the total power, and so its nonuniformities can be estimated by comparison with total power. Indeed, by fitting the power calculated from the full nonuniform model (solid line) to the sinusoid of best fit to the data (dotted line), we are able to deduce the profile of $G_{sn}\phi_n$, giving $G_{sn}\phi_n \approx 1.12 + 0.14 \sin(2\pi x/l_x + 5.2)$. This indicates that postsynaptic subthalamic input to relay nuclei is approximately 25% greater at the back of the head than at the front, or volume conduction is 25% less, or some combination of both. We cannot at this stage distinguish between these alternatives.

V. AN APPLICATION: OCCIPITAL ALPHA DOMINANCE

In the previous section we fitted the local effective value (LEV) model to experimental spectra to infer likely parameter trends across the head. We now incorporate these trends into the nonuniform model to investigate the spatial variation of the eyes-closed spectrum. We pay particular attention to

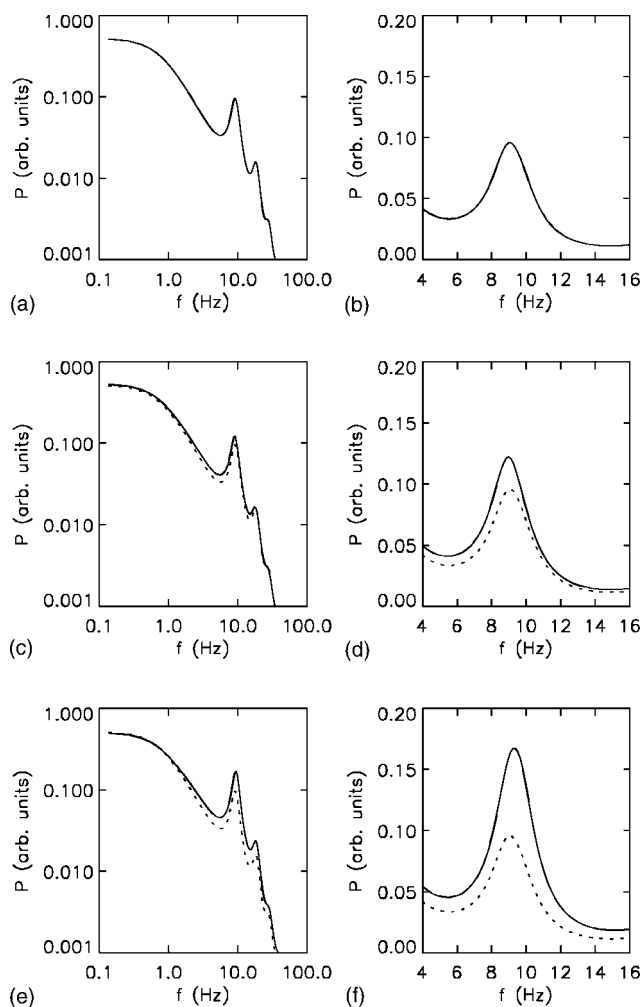


FIG. 11. Local spectra predicted by the model from the parameter variations in Fig. 9, on log-log (first column) and log-linear (second column) scales. The solid line in each panel represents the local spectrum at the front of the head [(a) and (b)], the center of the head [(c) and (d)], and the back of the head [(e) and (f)]. The spectrum at the front of the head is overplotted for comparison as a dotted line in panels (c)–(f).

one possible application of the present work: examining the phenomenon of occipital dominance of the alpha rhythm.

The solid lines in Fig. 11 show the locally measured spectra predicted from the nonuniform model at three points across the head. The top row is at $d=0$ m (the front of the head), the middle row is at $d=0.2$ m, and the bottom row is at $d=0.4$ m (the back of the head). The spectra at the front of the head are also shown for comparison as dotted lines in the bottom two rows. In each case, the left column shows the spectrum from 0.25 to 50 Hz on a log-log scale and the right column shows the alpha peak magnified on a log-linear scale.

We see that the alpha power increases only slightly from the front to the center of the head, then increases by a factor of approximately two towards the back of the head. The log-log plots show that the power at low frequencies remains relatively constant across the head, in agreement with published data [2,23,24]. Power at the beta frequency (≈ 20 Hz) is seen to increase occipitally in Fig. 11; this

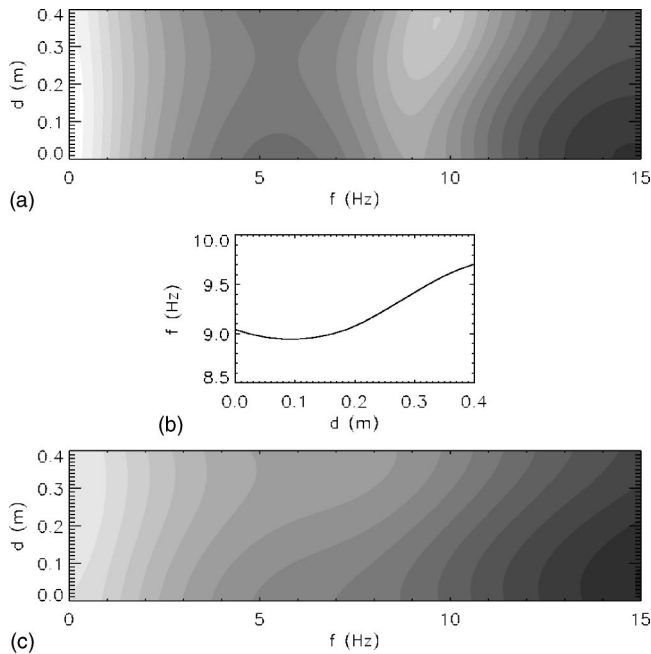


FIG. 12. Spectral variation across the head as a function of both position and frequency, where $d=0$ m is the front of the head, and $d=0.4$ m is the back of the head. Light shades represent high power and dark shades represent low power; the gray scale spans two orders of magnitude. Panel (a) represents an eyes-closed state, using the coefficients a shown in Table I, and panel (c) represents an eyes-open state, using parameters estimated from physiology and fitting the model to data. Panel (b) shows the variation of the alpha peak frequency across the head, for the eyes-closed state.

agrees with the findings of some authors [24], although an occipital beta power increase was not reported in some studies with fewer subjects [2], however, their data were consistent with such a trend. In typical studies, the data around the beta peak is binned over a total bandwidth of ≈ 20 Hz, so beta-specific trends may be obscured in any case.

Figure 12 shows the spectral variation of the predicted spectrum across the head as a contour map of power, in which light shades represent high power and dark shades represent low power. As previously, the front of the head is at $d=0$ m, and the back of the head is at $d=0.4$ m. Panel (a) is for the nonuniform eyes-closed parameters as above, and clearly demonstrates the spectral peaks at low frequencies and at approximately 10 Hz. Furthermore, the occipital increase in the peak alpha power is strongly apparent, as is the relative site invariance of power at other frequencies; note that the greatest alpha power does not occur at the very back of the head, but at $d \approx 0.37$ m. Let us consider now the predicted frequency of the alpha peak for the eyes-closed parameters. This peak frequency was measured from the predicted spectrum, and is shown in panel (b). The peak frequency is relatively invariant over the front half of the head, at approximately 9 Hz. The frequency then increases smoothly towards the back of the head, reaching 9.7 Hz at $d=0.4$ m. This agrees quantitatively with previously quoted decreases of 0.5–1.0 Hz at the front of the head compared to the back [1]. Thus our corticothalamic model shows that alpha-like rhythms at the front of the head can be generated by

the same mechanism (corticothalamic loop resonances) responsible for the alpha rhythms at the back of the head, and should therefore be considered to be part of the same phenomenon. Furthermore, the lower amplitude and frequency in frontal regions, which have historically sometimes been used to argue against frontal rhythms being termed “alpha” [1], can be accounted for by moderate sinusoidal variations in parameters across the brain. In particular, with reference to Eq. (18), we confirm that the frontal decrease in alpha frequency is largely due to the occipital increase in corticothalamic delay t_0 , as previously proposed [10]. In addition, we propose that the occipital increase in power is due to an occipital increase in thalamic gains, and concurrent decrease in cortical gains.

Figure 12(c) illustrates the spatial variation of the spectrum for an eyes-open state, in which the alpha power does not dominate, and the spectrum is relatively featureless. The nominal parameters for this state have been estimated from extensive modeling, fitting the model spectrum to data obtained from 100 normal subjects, and consideration of anatomical and physiological detail [20,28]; its location in the state space is shown in Fig. 3. For the purposes of this illustration, the nonuniformities in each of the eyes-open parameters have been assumed to have the same phase and relative amplitude as those for eyes closed. We see that the power at all frequencies is largely independent of position on the head for the eyes open spectrum, except for a slight frequency-independent occipital increase, in agreement with observation.

VI. DISCUSSION AND CONCLUSIONS

This paper had three main aims: to determine the extent to which local activity in the brain can be approximated by using a uniform model; to ascertain likely front-to-back spatial nonuniformities in the model parameters using data obtained from 98 normal subjects; and, to use these insights to study one application, namely to understand the physiological and anatomical causes of the increased power and frequency of the alpha rhythm in occipital regions compared to frontal ones.

With regard to the first of the above aims, comparisons between uniform and nonuniform parameter profiles indicated that at certain frequencies, local cortical activity is indeed affected by dynamics at distant sites: for low frequencies ($f \lesssim 2$ Hz), the local dynamics are dependent on low-wave-number activity at distant sites, as reflected in the dispersion relation; at the alpha frequency, signal propagation is inherently weakly damped, so low-wave-number activity elsewhere can contribute moderately to the local spectrum. At these frequencies, the local spectrum is affected in a largely predictable way; for example, if the mean magnitude of a parameter is lower than its local magnitude, then its form will change in the same direction as if its effective local magnitude had been reduced. Thus if the local magnitude equals the mean magnitude, then the local nonuniform spectrum is very similar to the mean (global) uniform spectrum, with only minor differences due to mode coupling. Some model parameters, such as the damping γ_e and dendritic de-

lay α , do not affect low-frequency activity significantly, and can be treated at each point on the head as being independent of their values elsewhere to a good approximation. For all parameters, this type of local independence can be assumed to a first approximation.

We next determined the effect on the spectrum of varying the parameters simultaneously. For the illustrative case presented in Fig. 8, in which the parameters varied all shared the same profile, much of the low-frequency discrepancy between the LEV and nonuniform spectra canceled out, due to competing effects from the different parameters. In general, if the sum of the state parameters x and y remains approximately constant across the head, the low-frequency discrepancy between the LEV and nonuniform spectra tends to cancel, and the local approximation remains valid. We remark that an anomalous case in which the parameters do not covary might well violate the local approximation, especially at low frequencies; in such a case, the full nonuniform spectrum should be fitted to the data to accurately deduce the parameter profiles. In general, we found that the local effective value (LEV) spectrum provides a good approximation to the fully nonuniform one, when the parameter nonuniformities are of low order, with $\lambda \geq (4-5)r_e$, or $k \leq 15-20 \text{ m}^{-1}$. Finer scale details are averaged out in any case, due to volume conduction through the skull, which is significant for $k \leq 15 \text{ m}^{-1}$ [7,20].

The second aim of this work was to estimate likely front-to-back variations in the model's physiological and anatomical parameters. For each parameter, a sinusoid of fixed period, representing the first Fourier component of the modal decomposition, was found to be a good model for the spatial nonuniformity inferred from the inverse modeling of 98 normal subjects; that is, the nonuniformities were found to be of low order, indicating that a local approximation (LEV) is likely to adequately model local activity. Three coefficients were fitted to the data, representing the mean, amplitude, and phase of the sinusoid. For each parameter, the mean agreed with previously estimated mean values [20,28], while the amplitude and phase represent the nonuniformities. We discuss these in terms of physiology and anatomy in paragraphs (i)–(vi) below. Note that for each parameter, the trend is a mean over 98 subjects; the trend in an individual subject may differ from this mean.

(i) Let us consider first the variations in the intracortical gains G_{ee} and G_{ei} . This work implies that G_{ee} and G_{ei} have largest magnitude prefrontally, as shown in Figs. 9(a) and 9(b). This trend could be a result of either more prolific, or stronger, intracortical connections in the frontal lobes, reflecting their role in planning and abstract thought. The visual cortex, located occipitally, has the most excitatory recurrent connectivity of any cortical area; however, previous work using the uniform version of this model has shown that the relatively short-scale recurrent excitatory connections may not be very important in determining the frequency spectrum in the model, with an exception in the case of evoked response potentials [5]. We deduce that the trend inferred from this work in which G_{ee} and G_{ei} have largest magnitude prefrontally, is likely due to stronger, or more prolific long-range intracortical connections in the frontal lobes. That the two have a similar phase and hence vary

together is significant, since the competing excitatory and inhibitory effects must balance for the brain's activity to remain stable; this is reflected in their influence over the cortical state parameter x . Furthermore, Figs. 7(a) and 7(b) indicate that the local approximation is likely to be good, since the low-frequency discrepancies between the LEV and nonuniform spectra for these parameters would cancel. Table I implies that the nonuniformities in G_{ee} and G_{ei} have amplitudes of $\approx 28\%$ and 20% of their nominal values, respectively. However, these values were obtained using the LEV model, and are hence "effective" local values; the relative amplitudes of the nonuniformities may be slightly larger than quoted above, although, as stated, their competing discrepancies at low frequencies would largely cancel out, and there are few discrepancies elsewhere.

(ii) Let us consider now the corticothalamic and intrathalamic gains G_{ese} , G_{esre} , and G_{srs} . As with the cortical gains, G_{ese} and G_{srs} have similar phases, as seen in Figs. 9(c) and 9(e), indicating that low-frequency discrepancies between the LEV and nonuniform spectra, seen in Figs. 7(c)–7(e) would tend to cancel out, so the local approximation remains valid. Furthermore, the similarity of the phases enables their competing effects at low frequencies to balance, thereby maintaining cortical stability, as reflected in Eq. (17). In general all three gain parameters increase towards the back of the head. The similarity of the phases indicates that shared anatomical structures are likely responsible for their nonuniformities. Anatomical measurements in the thalamus of neuronal density in various sensory relay nuclei [29], limbic relay nuclei [30], motor relay nuclei [31], prefrontal relay nuclei [32], and association relay nuclei [33], indicate that the lateral geniculate nucleus (LGN, which relays input from the retina to the visual cortex) has the highest neuronal density, varying from $(1.5-3) \times 10^4 \text{ mm}^{-3}$ compared to $(0.5-1.3) \times 10^4 \text{ mm}^{-3}$ across the other thalamic regions. Thus one might expect signals which pass through the LGN, which is located occipitally, to be larger than those which pass through less dense regions of the thalamus. Consider now the reticular thalamic nucleus (RTN), shown in Fig. 2. Towards the back of the RTN, the cells tend to be elongated and larger than at the front [34–36], so we might expect signals which pass through the back of the RTN to be stronger than those which pass through the front. Thus the findings of increased occipital thalamic gains in the present work are consistent with anatomical measurements. Table I implies that the nonuniformities in G_{ese} , G_{esre} , and G_{srs} have amplitudes of ≈ 14 , 16 , and 36% of their nominal values, respectively. However, Fig. 7 shows that nonuniformities in these parameters affect the local spectrum via dispersion, which makes their effective local values nearer the mean than the actual local values; hence the amplitudes of the nonuniformities may be slightly larger than the quoted values.

(iii) The inverse-modeling routine did not directly fit the subthalamic input, $G_{sn}\phi_n$; its spatial nonuniformity was estimated by fitting the power calculated from the nonuniform model to the data. We found that the postsynaptic white-noise input to the back of the thalamus was about 25% greater than to the front, although some of the variation in power could be due to nonuniformities in the skull thickness, which alters the volume conduction through the head. We

would not expect skull thickness to vary between states of arousal; however, from physiology, we might expect the amplitude of the subthalamic input to do so.

(iv) In addition to the gains, the present work found nonuniformities in the signal damping rate $\gamma_e = v_e / r_e$. There was a significant occipital increase in γ_e , which enhances the occipital alpha dominance, with little effect at lower frequencies. The physiological implication is that either signal conduction velocity increases or mean excitatory (pyramidal) axon length decreases occipitally. Table I indicates that the nonuniformity in γ_e has a relative amplitude of $\approx 18\%$.

(v) Inverse modeling also indicated that there is a general decrease in the dendritic delay α towards the back of the head. The physiological implication is that synaptodendritic dynamics vary across the head, possibly due to nonuniform neurotransmitter actions. Decreases in α have previously been associated with decreased sensory processing [28], which is in turn associated with increased alpha frequency power [37]. Table I indicates that the nonuniformity in α has a relative amplitude of $\approx 14\%$.

(vi) The present work indicates that the corticothalamic loop propagation delay t_0 decreases sinusoidally towards the back of the head, with an amplitude of 3 ms. This result agrees quantitatively and qualitatively with the predictions of a previous investigation into split alpha peaks [10]. It is unclear what physiological mechanism is responsible for this decrease, since an initial study of path lengths indicates that the loop distance is in fact longer to the back of the head than to the front; however, an increase in propagation velocity v_e , such as that suggested by the increase in damping γ_e , would lead to an increase in the corticothalamic loop velocity [20], and would contribute to an occipital decrease in the loop delay t_0 . Table I indicates that the nonuniformity in t_0 has a relative amplitude of $\approx 4\%$.

The third aim of this work was to apply the nonuniform model to an existing problem: explaining the phenomenon of occipital alpha dominance, and determining its cause. Let us first turn our attention to other studies, which have mapped variations in alpha using various measures of cortical and subcortical activity. For example, a study using simultaneous recording of EEG and O^{15} -water positron emission tomography (PET) [15] found positive correlations between alpha activity and blood flow through the thalamus, midbrain, and parts of the limbic system. The study also found a negative correlation between alpha activity and blood flow through the occipital cortex and a portion of prefrontal cortex. In another study [16], simultaneous EEG and functional magnetic resonance imaging (fMRI) data were recorded to correlate changes in alpha activity with changes in blood oxygenation levels throughout the brain. This study also found alpha to be positively correlated with thalamic activity, and negatively correlated with cortical activity, particularly occipitally. Further EEG-fMRI studies also found negative correlations between occipital cortical blood oxygenation and alpha activity [16]. However, results from such studies are not always in agreement. For example, Larson *et al.* [13] and Lindgren *et al.* [14] investigated possible correlations between alpha activity and metabolic rate, using simultaneous EEG and fluoro-deoxyglucose PET imaging. Both found a negative correlation between thalamic metabolic rate and al-

pha activity in normal subjects, in contrast to the above studies. Neither Larson *et al.* nor Lindgren *et al.* recorded correlations with cortical metabolic rate.

Correlative studies such as those outlined above are unable to distinguish between regions which actively generate alpha, and regions in which activity is correlated with EEG alpha but not causally linked to it [16]. The model is not similarly constrained. We predict that the alpha rhythm is generated in the corticothalamic loop [3], and the present work indicates that variations in alpha power across the head are primarily due to variations in the feedback strengths through different parts of the loop, including the intracortical and intrathalamic parts. Specifically, our results indicate that occipital alpha dominance is due to a decrease in occipital cortical gains, and an increase in occipital thalamic gains, where an increased gain may indicate an increase in activity. This prediction is in agreement with four of the six studies outlined above [15,16]. We address the disagreement with the results of Lindgren *et al.* [14] and Larson *et al.* [13] by noting that PET does not have sufficient spatial resolution to distinguish between the different thalamic nuclei [13], and thus a gradient in thalamic activity such as the one implicated by the present work cannot be reliably captured by PET imaging; indeed, the thalamic fMRI study [16], which has sufficient spatial resolution, is in agreement with our results. None of the studies investigated the frequency of the alpha peak. We reiterate our earlier conclusion [10] that the increased alpha frequency at the back of the head arises largely from the decreased corticothalamic delay, possibly due to larger conduction velocity here; however, nonuniformities in this parameter alone are not sufficient to account for the observed occipital increase in alpha power. The same mechanism was found to produce alphalike activity across the head; we deduce that the alphalike rhythms at the front of the head are indeed part of the same phenomenon as their occipital counterpart.

A great advantage of the model is its ability to link EEG activity with the underlying physiology and anatomy. Indeed, we propose that occipital alpha dominance is largely due to the occipital increase in thalamic cell density and concurrent decrease in cortical connection strengths, as discussed above. The effect is likely heightened by specific parameter changes in the eyes-closed state; however, its dependence on neuronal density implies that the fronto-occipital gradient is not entirely dependent on brain state. However, significant occipital variation in the spectrum is not reported for the eyes-open state, for example. In an attempt to understand this apparent paradox, we applied nonuniformities with the same phase and relative amplitude to eyesopen parameters, and found very little consequent variation in power across the brain, apart from a frequency-independent increase towards the back. This is most likely due to the fact that the eyes-open state lies further from the instability boundaries than the marginally stable eyes-closed state, and so is less sensitive to slight variations in the state parameters x , y , and z . The model could be fitted to eyes-open data to determine whether the phase and relative amplitudes of the nonuniformities are the same as for eyes closed. If they were found to be similar, we could conclude with more confidence that the nonuniformities are indeed due largely to the topography of the under-

lying anatomy; the extent of the differences would provide an estimate of the importance of state-specific effects.

The present work has implications for the stability of the brain. In reference to Figs. 3 and 10 we see that nonuniformities place the back of the head nearer the alpha instability boundary than the front, especially in the eyes-closed condition. Thus, for eyes closed, it would be easier to cross the boundary into an unstable (e.g., epileptic) state from the back of the head, and one would expect alpha-frequency seizures to dominate here. This result may explain the occipital prevalence of seizures which are induced by eye closure [38–42]. Such seizures are most common in childhood, with a peak onset at age five [39], which can be explained in the context of the present work by the fact that children generally show a higher amplitude alpha rhythm than adults [1].

In an application, we have shown that our spatially nonuniform model of corticothalamic dynamics is able to quantitatively reproduce observed site-dependent variations in the

alpha rhythm. In particular, our results indicate that the phenomenon of occipital alpha dominance can be accounted for by low-order spatially nonuniform feedback from the corticothalamic loop, modulated by decreased cortical activity and increased thalamic activity in occipital regions compared to frontal ones. The inferred parameter nonuniformities agree with anatomical and physiological experiments, and with inverse modeling of 98 subjects' spectra. The nonuniform model has obvious potential applications in investigating diverse spatially specific phenomena, such as brain tumors and localized epileptic seizures.

ACKNOWLEDGMENTS

The authors thank C. J. Rennie and D. L. Rowe for stimulating discussions and valuable assistance with the inverse modeling code. This work was supported by a University of Sydney Sesqui Grant.

-
- [1] O. N. Markand, *J. Clin. Neurophysiol.* **7**, 163 (1990).
- [2] L. DeGennaro, M. Ferrara, G. Curcio, and R. Cristiani, *Clin. Neurophysiol.* **112**, 1901 (2001).
- [3] P. A. Robinson, C. J. Rennie, J. J. Wright, H. Bahramali, E. Gordon, and D. L. Rowe, *Phys. Rev. E* **63**, 021903 (2001).
- [4] P. A. Robinson, C. J. Rennie, and D. L. Rowe, *Phys. Rev. E* **65**, 041924 (2002).
- [5] C. J. Rennie, P. A. Robinson, and J. J. Wright, *Biol. Cybern.* **86**, 457 (2002).
- [6] P. A. Robinson, *J. Theor. Biol.* **222**, 163 (2003).
- [7] S. C. O'Connor, P. A. Robinson, and A. K.I. Chiang, *Phys. Rev. E* **66**, 061905 (2002).
- [8] S. C. O'Connor and P. A. Robinson, *Phys. Rev. E* **67**, 051912 (2003).
- [9] S. C. O'Connor and P. A. Robinson (unpublished).
- [10] P. A. Robinson, R. W. Whitehouse, and C. J. Rennie *Phys. Rev. E* **68**, 021922 (2003).
- [11] E. Niedermeyer and F. H. Lopes da Silva, *Electroencephalography: Basic Principles, Clinical Applications, and Related Fields*, 4th Ed. (Williams & Wilkins, Baltimore, 1999).
- [12] P. L. Nunez, *Neocortical Dynamics and Human EEG Rhythms* (Oxford, New York, 1995).
- [13] C. L. Larson, R. J. Davidson, H. C. Abercrombie, R. T. Ward, S. M. Schaefer, D. C. Jackson, J. E. Holden, and S. B. Perlman, *Psychophysiology* **35**, 162 (1998).
- [14] K. A. Lindgren, C. L. Larson, S. M. Schaefer, H. C. Abercrombie, R. T. Ward, T. R. Oakes, J. E. Holden, S. B. Perlman, R. M. Benca, and R. J. Davidson, *Biol. Psychiatry* **45**, 943 (1999).
- [15] N. Sadato, S. Nakamura, T. Oohashi, E. Nishina, Y. Fuwamoto, A. Waki, and Y. Yonekura, *NeuroReport* **9**(5), 893 (1998).
- [16] R. I. Goldman, J. M. Stern, J. Engel, Jr., and M. S. Cohen, *NeuroReport* **13**(18), 2487 (2002).
- [17] S. C. O'Connor and P. A. Robinson, *Neurocomputing* **58-60C**, 1181 (2004).
- [18] P. A. Robinson, P. N. Loxley, S. C. O'Connor, and C. J. Rennie, *Phys. Rev. E* **63**, 041909 (2001).
- [19] C. J. Rennie, P. A. Robinson, and J. J. Wright, *Phys. Rev. E* **59**, 3320 (1999).
- [20] P. A. Robinson, C. J. Rennie, D. L. Rowe, and S. C. O'Connor, *Hum. Brain Mapp* **23**, 53 (2004).
- [21] P. A. Robinson, C. J. Rennie, and D. L. Rowe, *Phys. Rev. E* **65**, 041924 (2002).
- [22] P. L. Nunez, *Electric Fields of the Brain: The Neurophysics of EEG* (Oxford, New York, 1981).
- [23] B. Clemens, G. Sziget, and Z. Barta, *Epilepsy Res.* **42**, 105 (2000).
- [24] V. Knott, C. Mahoney, S. Kennedy, and K. Evans, *Psychiatry Res.: Neuroimaging* **106**, 123 (2001).
- [25] H. Bahramali, E. Gordon, J. Lagopoulos, C. L. Clim, W. Li, J. Leslie, and J. Wright, *Exp. Aging Res.* **25**, 69 (1999).
- [26] G. Gratton, M. Coles, and E. Donchin, *Electroencephalogr. Clin. Neurophysiol.* **55**, 168 (1983).
- [27] W. H. Press, S. A. Teukolsky, W. T. Vetterling, and B. P. Flannery, *Numerical Recipes in C* (Cambridge University Press, New York, 1992).
- [28] D. L. Rowe, P. A. Robinson, C. J. Rennie, and R. C. Powles (unpublished).
- [29] E. Armstrong, *Am. J. Phys. Anthropol.* **51**, 365 (1979).
- [30] E. Armstrong, *Am. J. Phys. Anthropol.* **52**, 43 (1980).
- [31] E. Armstrong, *Am. J. Phys. Anthropol.* **52**, 405 (1980).
- [32] A. J. Harding, G. M. Halliday, and K. Cullen, *J. Neurosci. Methods* **51**, 83 (1994).
- [33] E. Armstrong, *Am. J. Phys. Anthropol.* **55**, 369 (1981).
- [34] E. G. Jones, *J. Comp. Neurol.* **162**, 285 (1975).
- [35] A. E. Clemence and J. Mitrofanis, *J. Comp. Neurol.* **322**, 167 (1992).
- [36] *Thalamus Volume I: Organisation and Function*, edited by M. Steriade, E. G. Jones, and D. A. McCormick (Elsevier, Oxford, 1997).
- [37] C. Shagass, in *Handbook of Psychophysiology*, edited by N. S. Greenfield and R. A. Sternbach (Rinehart and Winston, New York, 1972).

- [38] R. G. Bittar, F. Andermann, A. Olivier, F. Dubeau, D. O. Dumoulin, G. B. Pike, and D. C. Reutens, *Epilepsia* **40**, 170 (1999).
- [39] C. P. Panayiotopoulos, *Arch. Dis. Child* **78**, 3 (1998).
- [40] C. P. Panayiotopoulos, *J. Neurol., Neurosurg. Psychiatry* **66**, 536 (1999).
- [41] A. Verrotti, S. Domizio, D. Melchionda, M. Guerra, T. Mucedola, M. Onofri, F. Chiarelli, and G. Sabatino, *Childs Nerv. Syst.* **16**, 35 (2000).
- [42] C. Kurth, H. J. Bittermann, V. Wegerer, S. Bleich, and B. J. Steinhoff, *Epilepsia* **42**, 497 (2001).